LBL-299
c.2

THREE-COMPONENT ION-EXCHANGE IN FIXED BEDS APPLICATION TO PRE-TREATMENT OF SALINE-WATER EVAPORATOR FEED

Angelo Giuliano Sassi,* Gerhard Klein,
and Theodore Vermeulen

December 1971

AEC Contract No. W-7405-eng-48

*Filed as an M.S. Thesis

TWO-WEEK LOAN COPY

This is a Library Circulating Copy which may be borrowed for two weeks. For a personal retention copy, call Tech. Info. Division, Ext. 5545

LAWRENCE BERKELEY LABORATORY • UNIVERSITY OF CALIFORNIA • BERKELEY

LBL-299
c.2

DISCLAIMER

This document was prepared as an account of work sponsored by the United States Government. While this document is believed to contain correct information, neither the United States Government nor any agency thereof, nor the Regents of the University of California, nor any of their employees, makes any warranty, express or implied, or assumes any legal responsibility for the accuracy, completeness, or usefulness of any information, apparatus, product, or process disclosed, or represents that its use would not infringe privately owned rights. Reference herein to any specific commercial product, process, or service by its trade name, trademark, manufacturer, or otherwise, does not necessarily constitute or imply its endorsement, recommendation, or favoring by the United States Government or any agency thereof, or the Regents of the University of California. The views and opinions of authors expressed herein do not necessarily state or reflect those of the United States Government or any agency thereof or the Regents of the University of California.

THREE-COMPONENT ION-EXCHANGE IN FIXED BEDS
APPLICATION TO PRE-TREATMENT OF SALINE-WATER EVAPORATOR FEED

Angelo Giuliano Sassi, Gerhard Klein, and Theodore Vermeulen

Lawrence Berkeley Laboratory
University of California
Berkeley, California 94720

December 1971

THREE-COMPONENT ION-EXCHANGE IN FIXED BEDS

APPLICATION TO PRE-TREATMENT OF SALINE-WATER EVAPORATOR FEED

TABLE OF CONTENTS

	Page No.
LIST OF FIGURES	v
LIST OF TABLES	ix
ABSTRACT	xi
I. INTRODUCTION	1
II. THEORY	3
A. Equilibrium Behavior	3
B. Rate Behavior	29
III. APPLICATION	42
A. Equilibrium Behavior	42
B. Rate Behavior	64
IV. SUMMARY AND CONCLUSIONS	93
ACKNOWLEDGMENT	95
NOMENCLATURE	96
REFERENCES	99

LIST OF FIGURES

No.	Caption	Page No.
1	MASS-ACTION EQUILIBRIUM FOR THE BINARY SYSTEM CALCIUM(=A) - SODIUM(=C), AT C_o=0.62 N, WITH $K_{AC}Q/C_o$ = 8.06	5
2	MASS-ACTION EQUILIBRIUM FOR THE BINARY SYSTEM MAGNESIUM(=B) - SODIUM(=C) AT C_o=0.62 N, WITH $K_{BC}Q/C_o$ = 3.71	6
3	CONSTRUCTION OF THE ISOTHERM FOR A PARTIAL CHANGE IN EQUILIBRIUM CONCENTRATIONS BETWEEN (x',y') AND (x",y")	9
4	(a) MASS-ACTION EQUILIBRIUM FOR THE TERNARY SYSTEM CALCIUM(=A) - MAGNESIUM(=B) - SODIUM(=C) ON DUOLITE C-25 COMPOSITION PATHS FOR SEA-WATER SOFTENING BY ION-EXCHANGE: (b) COLUMN INITIALLY IN SODIUM FORM (c) COLUMN UNIFORMLY PRESATURATED WITH MAGNESIUM AND SODIUM IONS (d) COLUMN UNIFORMLY PRESATURATED WITH CALCIUM, SODIUM, AND MAGNESIUM IONS	12
5	EXAMPLE OF COMPOSITION-PATH GRID. SOLID LINES ARE 1,2 PATHS; DASHED LINES ARE 2,3 PATHS	24
6	SCHEMATIC CONCENTRATION-PROFILE AND ZONE-BOUND DESIGNATIONS FOR ABRUPT TRANSITION 1,2 AND GRADUAL TRANSITION 2,3	26
7	SCHEMATIC EFFLUENT-CONCENTRATION HISTORY AND ZONE-BOUND DESIGNATIONS FOR GRADUAL TRANSITION 2,3 AND ABRUPT TRANSITION 1,2	27
8	EFFECTS OF PÉCLET GROUP, PARTITION RATIO, AND DIFFUSIVITY RATIO ON HEIGHT OF A REACTION UNIT	36
9	CROSS-PLOT OF THROUGHPUT RATIO AT X = 0.90 AGAINST EQUILIBRIUM PARAMETER	39
10	DIMENSIONLESS MIDPOINT SLOPE AS A FUNCTION OF EQUILIBRIUM PARAMETER AND OF NUMBER OF REACTION UNITS	41

11 SEA-WATER SOFTENING BY A COLUMN UNIFORMLY PRESATURATED WITH CALCIUM, MAGNESIUM, AND SODIUM IONS: CALCIUM AND MAGNESIUM EFFLUENT-CONCENTRATION HISTORIES FOR RUN 4S 48

12 SEA-WATER SOFTENING BY COLUMN INITIALLY IN SODIUM FORM: CALCIUM AND MAGNESIUM EFFLUENT-CONCENTRATION HISTORIES FOR RUN 21S 49

13 PREDICTED PLATEAUS AND TRANSITIONS COMPARED TO EXPERIMENTAL CALCIUM AND MAGNESIUM EFFLUENT-CONCENTRATION HISTORIES FOR RUN 4S; REGENERATION BY FOUR TIMES CONCENTRATED BRINE 57

14 PREDICTED PLATEAUS AND TRANSITIONS COMPARED TO EXPERIMENTAL CALCIUM AND MAGNESIUM EFFLUENT-CONCENTRATION HISTORIES FOR RUN 21S; COLUMN INITIALLY IN SODIUM FORM 58

15 RESIN REGENERATION BY SODIUM IN COLUMN UNIFORMLY PRESATURATED WITH SEA WATER: CALCIUM AND MAGNESIUM EFFLUENT-CONCENTRATION HISTORIES FOR RUN 1RA 60

16 PREDICTED PLATEAUS AND TRANSITIONS (SOLID LINES) COMPARED TO EXPERIMENTAL CALCIUM AND MAGNESIUM EFFLUENT-CONCENTRATION HISTORIES FOR RUN 1RA; REGENERATION BY TWICE-CONCENTRATED BRINE 62

17 RESIN REGENERATION BY FOUR TIMES CONCENTRATED BRINE IN COLUMN UNIFORMLY PRESATURATED WITH SEA WATER. PREDICTED PLATEAUS AND TRANSITIONS (SOLID LINES) COMPARED TO EXPERIMENTAL CALCIUM EFFLUENT-CONCENTRATION HISTORY FOR RUN 3R 63

18 AMOUNT OF CALCIUM (SHADED AREA) IN THE EFFLUENT AFTER COMPLETE SATURATION OF COLUMN WITH SEA WATER; SCHEMATIC 66

19 AMOUNT OF CALCIUM (SHADED AREA) IN THE EFFLUENT AFTER REGENERATION OF THE COLUMN WITH CONCENTRATED BRINE; SCHEMATIC 67

20 PREDICTED AMOUNT OF CALCIUM (SHADED AREA) IN THE EFFLUENT AFTER COMPLETE SATURATION OF COLUMN WITH SEA WATER; SCHEMATIC 69

21 PREDICTED AMOUNT OF CALCIUM (SHADED AREA) IN THE EFFLUENT AFTER REGENERATION OF COLUMN WITH CONCENTRATED BRINE; SCHEMATIC 70

22 MATCH OF NORMALIZED CALCIUM 1,2-TRANSITION TO GENERALIZED REACTION-KINETIC BINARY MASTER CURVES FOR RUN 4S 74

23 MATCH OF NORMALIZED CALCIUM 1,2-TRANSITION TO GENERALIZED REACTION-KINETIC BINARY MASTER CURVES FOR RUN 21S 75

24 EFFECT OF MASS-TRANSFER RATES ON CALCIUM BREAKTHROUGH CURVES FOR EACH TRANSITION (REGENERATION WITH TWICE-CONCENTRATED BRINE) 76

25 MATCH OF NORMALIZED CALCIUM 1,2-TRANSITION TO GENERALIZED REACTION-KINETIC BINARY MASTER CURVES FOR RUN 1RA 79

26 EFFECT OF MASS-TRANSFER RATES ON CALCIUM BREAKTHROUGH CURVES FOR EACH TRANSITION (REGENERATION WITH FOUR TIMES CONCENTRATED BRINE) 80

27 MATCH OF NORMALIZED CALCIUM 1,2-TRANSITION TO GENERALIZED REACTION-KINETIC BINARY MASTER CURVES FOR RUN 3R 82

28 COMPARISON OF EXPERIMENTAL RESULTS WITH GENERAL CORRELATION 87

29 CORRELATION OF NUMBER OF REACTION UNITS AND FLOW RATE FOR SATURATION RUNS 90

LIST OF TABLES

Table No.	Caption	Page No.
I	OPERATING CONDITIONS FOR EXPERIMENTAL RUNS	43
II-a	CALCULATED PLATEAU-ZONE COMPOSITIONS FOR SATURATION RUNS	51
II-b	CALCULATED PLATEAU-ZONE COMPOSITIONS FOR REGENERATION RUNS (n = 2)	52
II-c	CALCULATED PLATEAU-ZONE COMPOSITIONS FOR REGENERATION RUNS (n = 4)	53
III-a	THROUGHPUT-PARAMETER VALUES FOR SATURATION RUNS	54
III-b	THROUGHPUT-PARAMETER VALUES FOR REGENERATION RUNS (n = 2)	55
III-c	THROUGHPUT-PARAMETER VALUES FOR REGENERATION RUNS (n = 4)	56
IV	EMPIRICAL PARAMETERS *a* AND *b*	71
V	NUMBERS OF REACTION UNITS FROM GENERALIZED REACTION-KINETIC CURVES MATCHED TO EXPERIMENTAL CALCIUM BREAKTHROUGH CURVES	77
VI	ESTIMATED HEIGHTS OF REACTION UNITS AND PÉCLET NUMBERS FOR FLOW	85
VII	INDIVIDUAL STEP CONTRIBUTIONS TO APPARENT OVERALL MASS-TRANSFER RESISTANCE	92

ABSTRACT

The existing column-performance theory for multi-component ion exchange utilizes the local-equilibrium conditions to determine the limiting concentration profiles inside the column, and in the effluent. These profiles contain a series of constant-composition plateaus with intervening transitions; the total number of transitions between feed and presaturant is one less than the total number of components. The actual shapes of transitions can then be calculated from nonequilibrium theory.

Sea-water softening by ion-exchange as a pretreatment before distillation removes scale-forming calcium compounds. Regeneration of the exhausted ion-exchange resin can be carried out using reject evaporator-brine, two or four times as concentrated as sea water. In this report, sea-water softening is examined as a three-component system involving calcium, magnesium, and sodium ions.

Equilibrium theory is applied to this system for a number of experimental saturation and regeneration runs at different operating conditions. Reported effluent-concentration-histories, involving stoichiometric values of throughput parameter for each transition and limiting concentration levels of each plateau, are compared with the predicted plateaus and transitions.

The nonequilibrium or dynamic behavior is approximated by a binary system in which a sodium-magnesium gross-ion counterdiffuses against calcium. The experimental calcium-concentration histories are matched to the theoretical binary master curves within the plateau-zone limits identified by equilibrium theory. The resulting numbers of reaction units (or values of mass-transfer coefficents) are used to identify internal diffusion as the machanism controlling the rate of mass-transfer. The contribution of fluid-phase pore diffusion to the mechanism of internal transport is found to be negligible compared to solid-phase diffusion. The results obtained for regeneration steps are found consistent with those for softening steps.

I. INTRODUCTION

Evaporation, one of the more important processes for economical conversion of sea water to fresh water, is performed in either vapor-recompression or multiple-effect heat transfer units. The inherent problem of precipitation of concentrated insoluble salts, or "scale", diminishes markedly its effectiveness and reliability of operation. In the proposed process, incoming sea water gives up considerable calcium and some magnesium to a strong-acid cation-exchange resin and then passes into the evaporation unit. The reject evaporator brine can serve as regenerant, because a shift in equilibrium resulting from increased total concentration now favors the displacement of divalent ions from the resin by sodium ions in the brine. This process has already been studied extensively at the Sea Water Conversion Laboratory of the University of California, in both theoretical and experimental aspects (2,12,13), and has been found to be feasible over a range of possible operating conditions.

Although the theory to interpret or predict such operation has become available, the experimental data obtained previously have not been examined fully in the light of this new theoretical knowledge. The purpose of

this study has been to compare experimental results with theoretical predictions, and thus to extract quantitative values of the governing mass-transfer coefficents, so that operating conditions can be optimized.

II. THEORY

A. Equilibrium Behavior

1. Binary Systems

Reversible binary ion exchange between a monovalent ion and a divalent ion may be expressed as a chemical reaction:

$$D^{+2} + 2RM = 2M^{+1} + R_2D \tag{1}$$

where R represents a stationary univalent exchange site on the resin. With the fluid-phase ion concentration c_i measured in milliequivalents per milliliter and the solid phase concentration q_i in milliequivalents per gram of dry resin, the equilibrium involved between D and M with R is represented approximately by an expression of the form

$$K_{DM} = \frac{q_D}{c_D}\left(\frac{c_M}{q_M}\right)^2 \tag{2}$$

obtained when the mass-action law (without activity corrections) is applied to Equation 1.

The total ion-equivalent concentration C_o and the total solid-phase capacity Q are constant for stoichiometric ion exchange, and are given by

$$c_M + c_D = C_o \; ; \; q_M + q_D = Q \tag{3}$$

Dimensionless concentrations (or equivalent fractions) can be constructed for each species

$$x_i = c_i/C_o \; ; \; y_i = q_i/Q \tag{4}$$

with

$$x_M + x_D = 1 \; ; \; y_M + y_D = 1 \qquad (5,6)$$

Substituting Equations 4 into Equation 2, and applying conditions 5 and 6, gives

$$\frac{K_{DM}Q}{C_o} = \underset{\sim}{K}_{DM} = \frac{y_D}{x_D}\left(\frac{1-x_D}{1-y_D}\right)^2 \qquad (7)$$

Here $\underset{\sim}{K}_{DM}$ is a dimensionless selectivity coefficient, which is approximately constant when Q and C_o are constant. It follows from Equation 7 that

$$\underset{\sim}{K}_{DM} = \frac{1}{\underset{\sim}{K}_{MD}} \qquad (8)$$

Where the selectivity coefficient is known for the binary system D-M at a constant temperature, Equation 7 shows that a single equilibrium value of the equivalent fraction of component D in the solid phase corresponds to each value of the equivalent fraction of D in the liquid phase. This solute equilibrium in the two phases may be depicted graphically by an "isotherm". Such equilibria are shown in Figures 1 and 2 for the two binary systems calcium-sodium and magnesium-sodium on Duolite C-25 resin (a macroporous polystyrene sulfonate), and Equation 7 for these systems becomes

$$\underset{\sim}{K}_{AC} = \frac{K_{AC}Q}{C_o} = \frac{y_A}{x_A}\left(\frac{1-x_A}{1-y_A}\right)^2 \qquad (9)$$

$$\underset{\sim}{K}_{BC} = \frac{K_{BC}Q}{C_o} = \frac{y_B}{x_B}\left(\frac{1-x_B}{1-y_B}\right)^2 \qquad (10)$$

where A, B, and C stand for calcium, magnesium and sodium respectively.

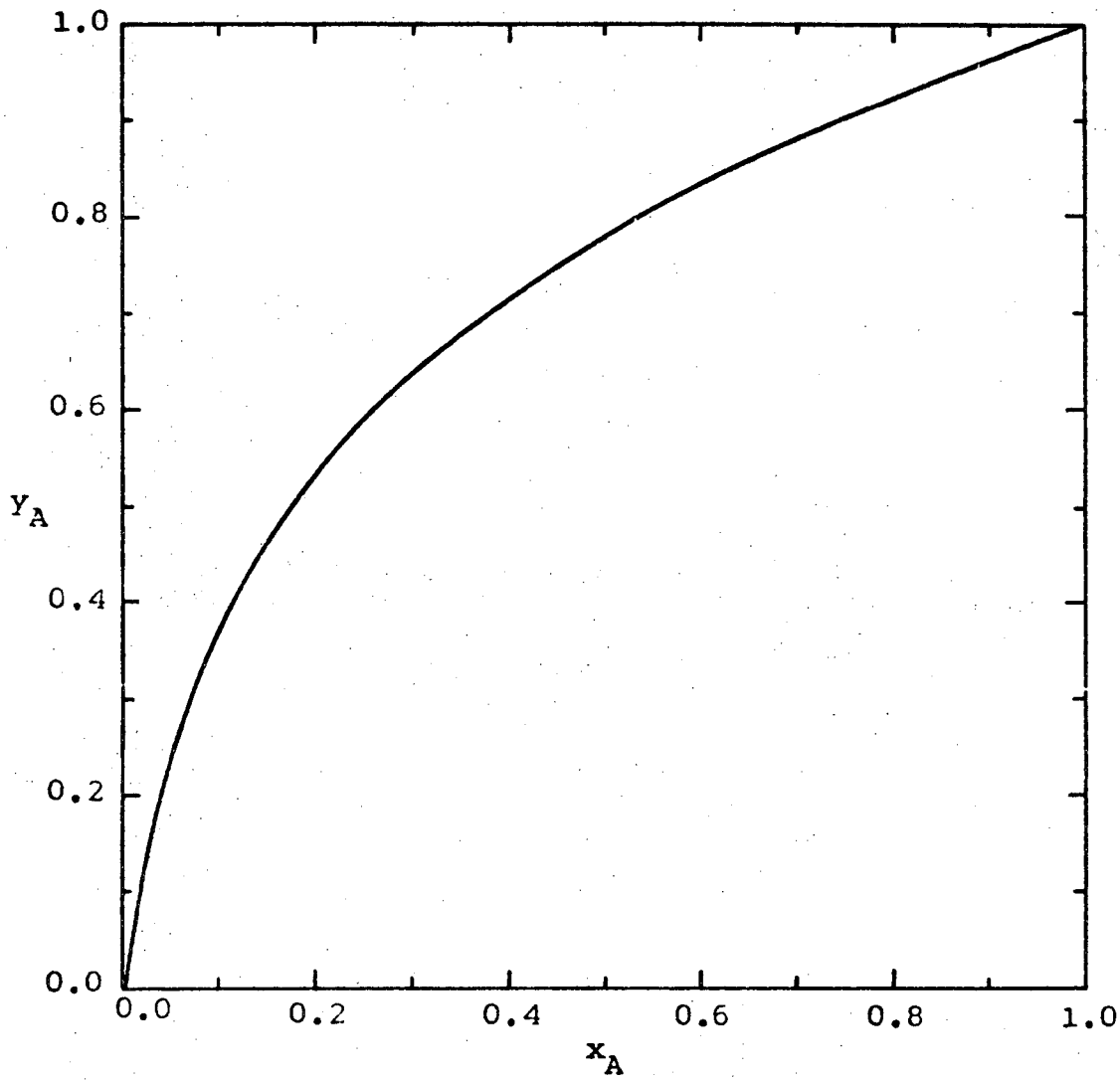

MASS-ACTION EQUILIBRIUM FOR THE BINARY SYSTEM CALCIUM(=A) - SODIUM(=C), AT C_o=0.62 N, WITH

$K_{AC}Q/C_o = 8.06$

FIGURE 1

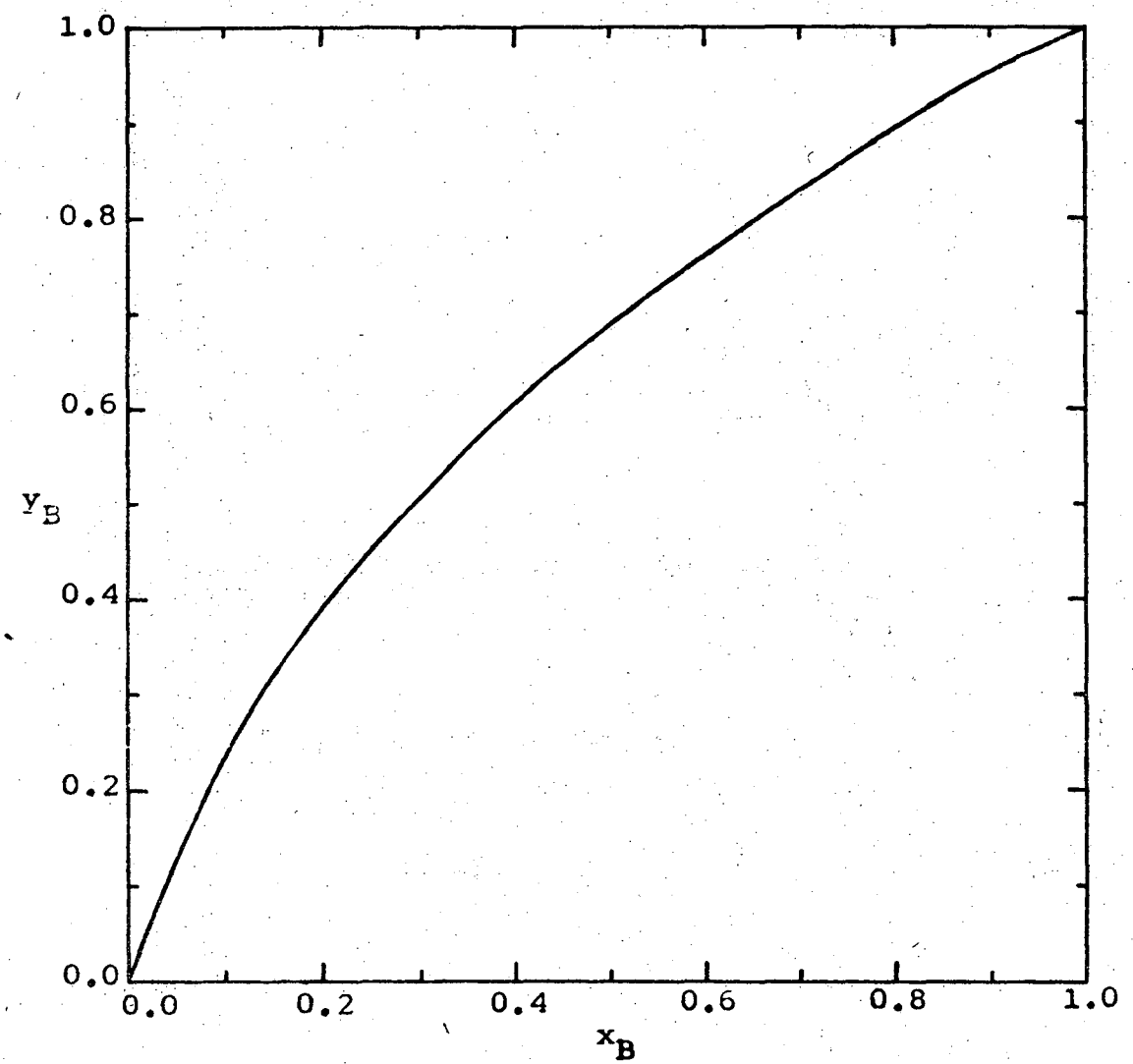

MASS-ACTION EQUILIBRIUM FOR THE BINARY SYSTEM MAGNESIUM(=B) - SODIUM(=C) AT C_o=0.62 N, WITH

$K_{BC}Q/C_o = 3.71$

FIGURE 2

For simplifying the binary mass-action case (Equation 7), an equilibrium parameter can be defined

$$r_{DM} = \frac{x_D(1-y_D)}{y_D(1-x_D)} = \frac{1}{r_{MD}} \tag{11}$$

Whenever such a parameter is applied to any particular ion-exchange process, it is analogous to the relative volatility or its reciprocal as used in distillation. Related to r_{DM}, the separation factor

$$\alpha_{DM} = \frac{1}{\alpha_{MD}} = \frac{y_D(1-x_D)}{x_D(1-y_D)} \tag{12}$$

is a generally used measure of the selectivity. Where the valences of the exchanging species are different, r_{DM} and α_{DM} vary with composition and can only approximate the true equilibrium over any given concentration range of interest.

The equilibrium parameter r_{DM} identifies the equilibrium increase in y from zero to unity that accompanies an increase in x from zero to unity. For a concentration change over only a part of the isotherm, a new equilibrium parameter R can be defined which identifies the equilibrium between Y and X (defined below), each ranging from zero to unity. As shown by Vermeulen and Hiester (3), the equilibrium parameter for a partial transition is

$$R = \frac{r + x' - rx'}{r + x'' - rx''} = \frac{X(1-Y)}{Y(1-X)} \tag{13}$$

where

$$X = \frac{x - x'}{x'' - x'} \; ; \; Y = \frac{y - y'}{y'' - y'} \qquad (14)$$

and x' (y') is the starting (downstream), and x" (y") the final (upstream), value of x (y).

Figure 3 shows the geometrical relation of the partial and total isotherms. As x' may be either larger or smaller than x", the partial change can occur either upward or downward.

2. Multicomponent Systems

For a binary system, Equation 7 expresses the functional relation

$$f(x_D, y_D) = 0 \qquad (15)$$

For a multicomponent system, then, a general expression for the equilibrium relationships between k exchangeable ion species and an exchanger may be written:

$$f_i(x_1, x_2, \ldots x_{k-1}, y_i) = 0 \qquad (16)$$

for each i in the range from i = 1 to i = k. The generalization of Equations 5 and 6 leads to

$$\sum_{i=1}^{k} x_i = 1 \quad \text{and} \quad \sum_{i=1}^{k} y_i = 1 \qquad (17,18)$$

Equation 17 indicates that it is sufficient to specify only k-1 x's in each equation; Equation 18 implies that there are only k-1 independent equations of the type of Equation 16.

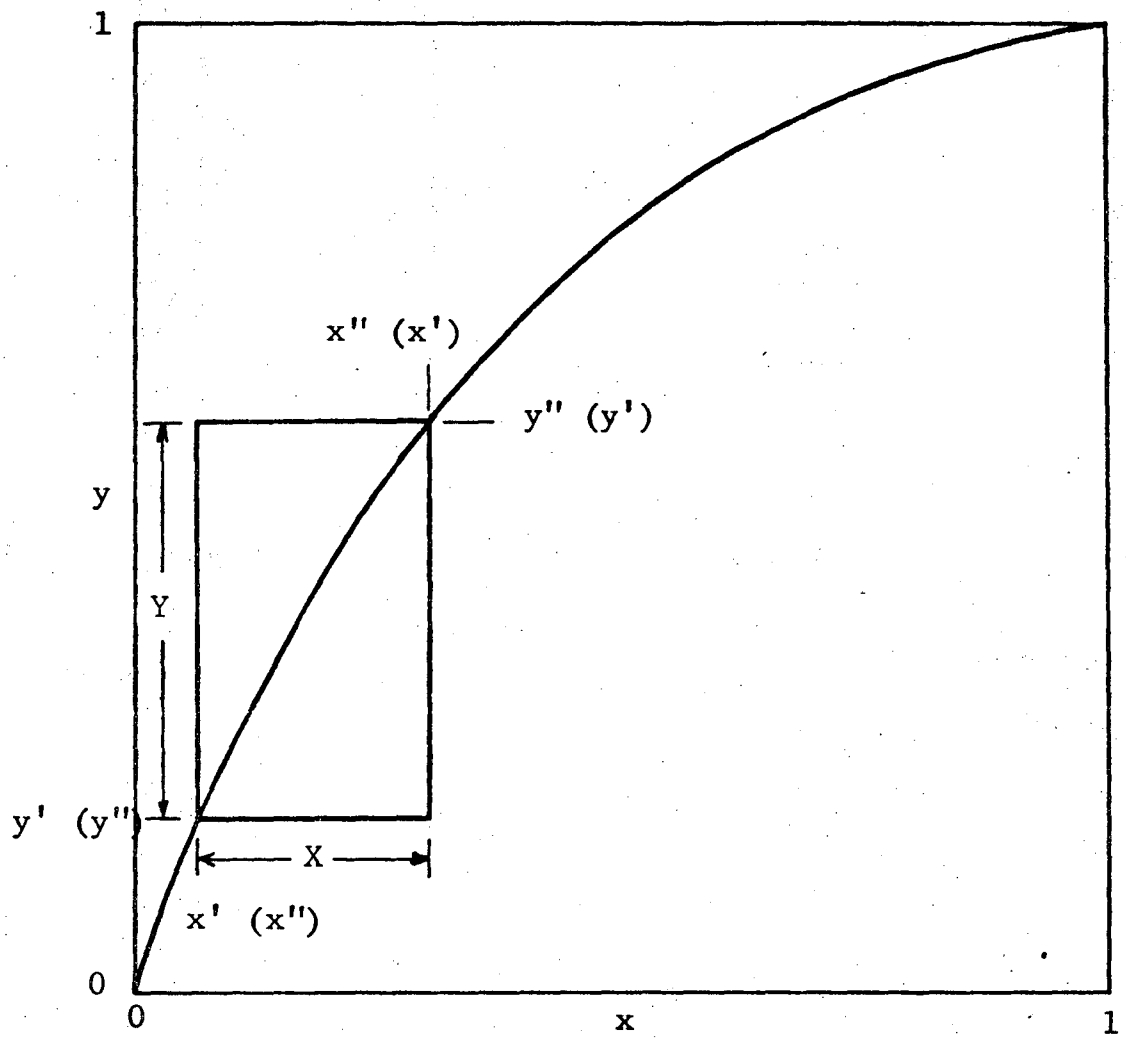

CONSTRUCTION OF THE ISOTHERM FOR A PARTIAL CHANGE IN EQUILIBRIUM CONCENTRATIONS BETWEEN (x',y') AND (x",y")

FIGURE 3

Thus, if a total of any k-1 concentration variables (either all x's or all y's) are specified, these with Equations 16, 17, and 18 will define the values of all the remaining concentrations in the system.

In many cases, the presence of other components does not affect significantly the equilibrium relationships between any two of the components. The isotherm can be expressed approximately in terms of k-1 independent equations of the type

$$f_{ij}(x_i, x_j, y_i, y_j) = 0 \tag{19}$$

where $i \neq j$. The equilibrium relationship most frequently used is the mass-action law discussed above; in the event that k-1 x's are specified, the k-th x is obtained by difference from unity, utilizing Equation 17. Where the $\underset{\sim}{K}_{ij}$ values are known, solution for the y's involves the equilibrium relations

$$y_j = x_j\left(\underset{\sim}{K}_{ji}\right)^{1/\nu_i}\left(\frac{y_i}{x_i}\right)^{\nu_j/\nu_i} \tag{20}$$

where ν_i is the absolute value of the valence of component i. For the three-component system calcium (=A) - magnesium (=B) - sodium (=C), the equations are:

$$\frac{K_{AC}Q}{C_o} = \frac{y_A}{x_A}\left(\frac{x_C}{y_C}\right)^2 \tag{21}$$

$$\frac{K_{BC}Q}{C_o} = \frac{y_B}{x_B}\left(\frac{x_C}{y_C}\right)^2 \tag{22}$$

$$x_A + x_B + x_C = 1 \tag{23}$$

$$y_A + y_B + y_C = 1 \tag{24}$$

Three-component isotherms can be represented on a triangular diagram. The regular grid of the diagram is used to represent the composition of one of the phases; the composition in the other phase is given by a set of contour lines, each corresponding to a constant concentration of one of the components. Figure 4a shows such a diagram for the variable-separation-factor equilibrium as characterized by Equations 21 and 22, for the system treated later in this report. For a constant separation factor, the contours become linear, as can be shown from the ternary isotherm equations (4).

3. Nomenclature

a. Partition Ratio. The dimensionless partition ratio is a useful equilibrium property and accounts for the total (or relative component) concentration level in each phase. For total concentration

$$\Lambda = \frac{Q\rho_b}{C_o} \tag{25}$$

where ρ_b is the mass of solid in its reference conformation per unit of solid plus fluid phase volume; $Q\rho_b$ thus is the total ion-equivalents of solutes per unit mixed volume; and C_o is the total ion-equivalents of solutes per unit fluid volume. For a concentration shift in systems corresponding to partially presaturated exchanger with mixed feed, the

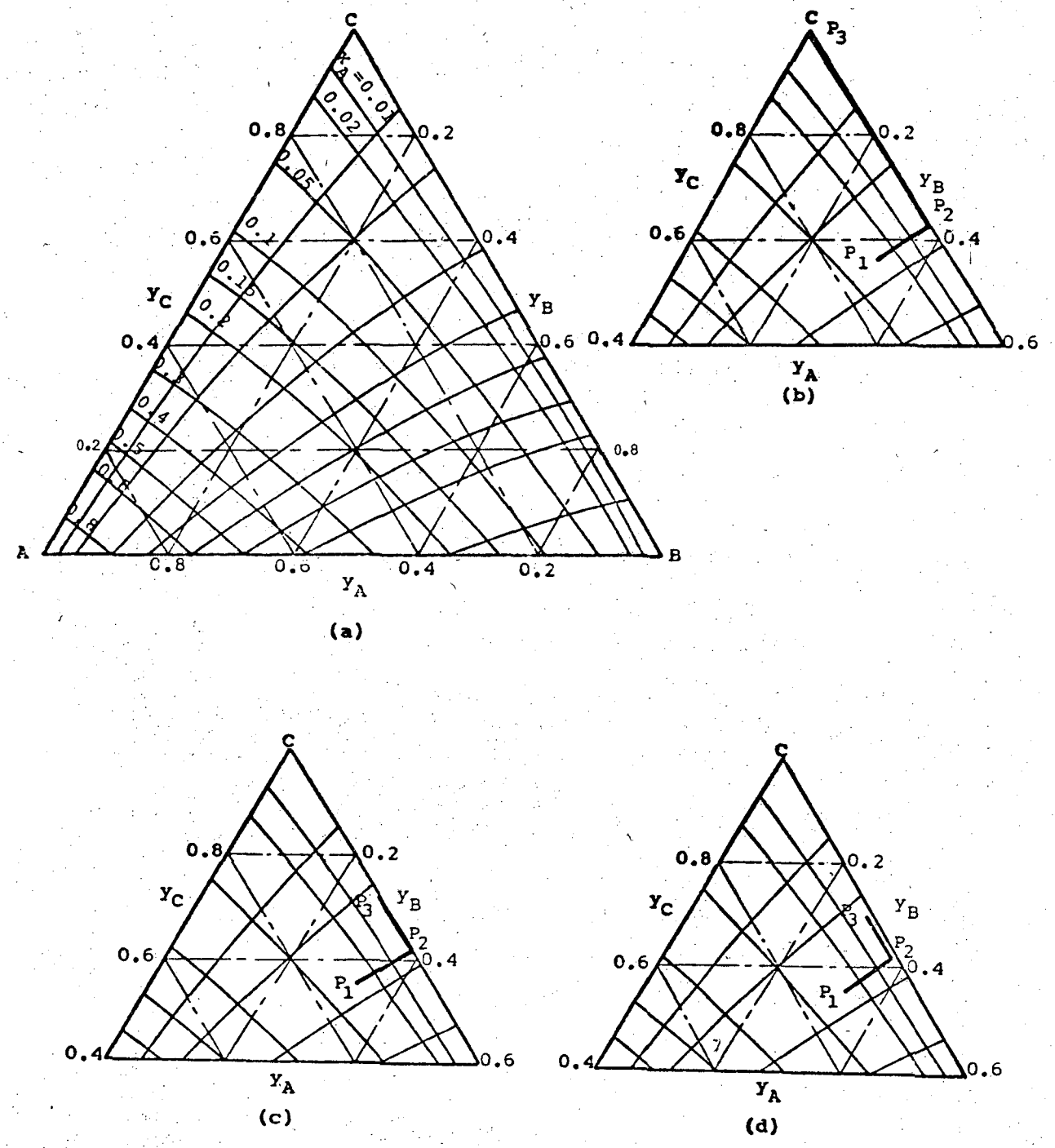

(a) MASS-ACTION EQUILIBRIUM FOR THE TERNARY SYSTEM CALCIUM(=A) - MAGNESIUM(=B) - SODIUM(=C) ON DUOLITE C-25
COMPOSITION PATHS FOR SEA-WATER SOFTENING BY ION-EXCHANGE:
(b) COLUMN INITIALLY IN SODIUM FORM
(c) COLUMN UNIFORMLY PRESATURATED WITH MAGNESIUM AND SODIUM IONS
(d) COLUMN UNIFORMLY PRESATURATED WITH CALCIUM, SODIUM, AND MAGNESIUM IONS

FIGURE 4

partition ratio applicable to the shift (transition) is

$$\underset{\sim}{\Lambda} = \frac{y'' - y'}{x'' - x'} \Lambda \tag{26}$$

b. Throughput Ratio. A general definition for the throughput ratio is

$$T = \frac{C_o(V - v\epsilon)}{Q \rho_b v} = \frac{V - v\epsilon}{\Lambda v} \tag{27}$$

where V is the volume of fluid fed to the column; v is the volume of the column and ϵ is the inter-particle void fraction; $v\epsilon$ is the void volume, or holdup of mobile fluid that has not travelled the full length at which T and v are being measured. The symbol $\underset{\sim}{T}$ refers to exchange between the actual limits and is given by the relation

$$\underset{\sim}{T} = T / \frac{y'' - y'}{x'' - x'} \tag{28}$$

4. Fixed-Bed Performance

A comprehensive study of multicomponent ion-exchange systems, using an equilibrium model in which local equilibrium exists at all times at each point of the exchanger bed, has been reported by Klein, Tondeur, and Vermeulen (4,6), who have shown that if an ion-exchange column contains a sufficient number of mass-transfer units (i.e., has sufficient length) to allow the concentration profile to develop fully, a total of n "plateau zones" of constant concentration will develop within the column if there are n exchanging ions, and if feed and presaturation concentrations are constant.

These plateau zones are separated by (n - 1) "transition zones" in which the concentration profile changes along the column at a fixed time.

The equilibrium theory is capable of predicting whether a transition zone will tend to exhibit constant-pattern or proportionate-pattern behavior, and of calculating the average throughput-parameter value $\bar{T}$ for each transition zone. In addition it provides the mathematical solution for calculating the concentrations of each species at each plateau zone for an n-component system having mass-action type isotherms; the two types of transition zones mentioned above, which have been identified in binary ion exchange, carry over to multicomponent systems, and are identified as follows:

a. Abrupt transition (corresponding to favorable equilibrium, for which the applicable equilibrium parameter R for the transition is less than unity). Such a transition is sharpening (tending toward a constant pattern, and thus occupying a steadily decreasing fraction of total liquid or solid volume involved).

b. Gradual transition (corresponding to unfavorable equilibrium, with R larger than unity). Such a transition is non-sharpening (tending toward a proportionate pattern)

The shape of a non-sharpening transition can often be determined approximately from equilibrium theory, whereas the true shape of a sharpening transition can only be determined by taking into consideration the kinetic behavior. The

"equilibrium" theory given below has the following limitations:

a. Local equilibrium exists at all times at each point of the bed.

b. Hydrodynamic mixing and diffusion in the flow direction are absent; that is, plug flow applies.

c. The bed is homogeneous.

d. Only beds uniformly presaturated with one or several components and receiving a feed of constant composition are considered.

e. Secondary processes, such as neutralization, weak-acid or weak-base formation in the fluid phase, complex formation, and precipitation, are assumed to be absent.

5. Characterization of Performance

The course of the operation of an ion-exchange column is usually described by an effluent-concentration history, that is, by the concentrations of the exchangeable ion species as a function of time or effluent volume. Under equilibrium conditions with uniform presaturation and constant feed composition, the time (measured from moment at which feed solvent reaches column outlet) or effluent-volume coordinate, for any given set of effluent concentrations, is proportional to the equivalents of feed solution that have passed through the column and inversely proportional to the number of equivalents of exchanger present, namely it is proportional to

the throughput parameter defined by Equation 27. A unique concentration history is thus obtained for a given ion-exchange material, feed, and initial exchanger composition. Use of the throughput parameter T makes it possible to combine the effects of volume, capacity, void fraction, and bulk density of the exchanger into a single term. Because equilibrium conditions prevail, the history is also independent of flow rate and bed depth. For each normalized effluent-concentration history, there is a corresponding sequence of unique normalized concentrations within the column obtained by representing the concentrations (y's and x's) as functions of 1/T.

6. Material Balances

For an infinitesimal column slice perpendicular to the direction of flow, through which an infinitesimal amount of solution is passing, the difference in the amounts of the ion species i that enter and leave the slice must be balanced by changes in the liquid- and solid-phase concentrations in the slice. This material balance, for each component, is expressed by:

$$\left(\frac{\partial x_i}{\partial v}\right)_V + \frac{Q\rho_b}{C_o}\left(\frac{\partial y_i}{\partial v}\right)_v + \epsilon\left(\frac{\partial x_i}{\partial v}\right)_v = 0 \qquad (29)$$

For continuous concentration changes, Equation 29 applies to any geometry and is not restricted to equilibrium operation. It is evident that solutions of the form

$$x_i = \text{constant} \; ; \; y_i = \text{constant} \qquad (30)$$

satisfy Equation 29 and correspond to a plateau-zone composition.

7. Gradual Transitions

For the case of uniform presaturation and constant feed composition, Sillén (7) has transformed Equation 29 into the ordinary differential equation

$$\left(\frac{dy_i}{dx_i}\right)_{path} = T \tag{31}$$

where T is defined by Equation 27 and $\left(\frac{dy_i}{dx_i}\right)_{path}$ is evaluated along a composition path followed throughout the transition. For set compositions of the plateau zones bounding the transition, this path, which must satisfy the isotherm, is unique.

8. Abrupt Transitions

Equation 31 does not describe the concentration discontinuities in abrupt transitions. Here it is replaced by Equation 32, given below. Formal application of Equation 31 to this case leads to concentration profiles which are "fictitious", in the sense that the plateau zones on either side of the concentration change are calculated to overlap during the transition. Material balance establishes the following relation between the concentration of any two components i and j in the plateau zone adjacent to a transition, either abrupt or gradual. For transition 1,2, between the intermediate and feed plateaus,

$$\frac{y_{i2} - y_{i1}}{x_{i2} - x_{i1}} = \frac{y_{j2} - y_{j1}}{x_{j2} - x_{j1}} = \bar{T}_{1,2} \tag{32}$$

An analagous expression for transition 2,3, between the pre-saturation and the intermediate plateaus, can be written by substituting index 1 with index 2, and index 2 with index 3. $\bar{T}$ is the stoichiometric value of the throughput parameter corresponding to the transition; and subscripts 1 and 2 refer to the upstream and downstream plateau zones, respectively. Equation 32 gives the stoichiometric center of every transition profile, whether real or fictitious, and $\bar{T}$ values for all components in any one transition must be identical.

9. Plateaus and Transitions in Three-Component Systems

Klein, Tondeur and Vermeulen (6) derived the following expression for a k-component system, applicable to a single transition in which n ($\leq$ k) components are present:

$$\sum_{i=1}^{n} \nu_i \frac{x_i y_i}{x_i T - y_i} = 0 \quad (x_i \neq 0,\ y_i \neq 0) \tag{33}$$

Equation 33 applies in each of the k plateau zones that develop, and has n-1 positive roots (6). Unless components are absent, the largest of these roots corresponds to compositions in the first transition zone; the next-to-the-largest root, to compositions in the second transition zone; etc. Calculations available for three-component systems with known equilibrium properties not equivalent to constant separation factors, have been developed for ion-exchange systems (8) with isotherms for each pair of solutes based on ideal mass-action relations in a general form equivalent to Equation 20:

$$(y_i/x_i)^{\nu_j}(x_j/y_j)^{\nu_i} = \underset{\sim}{K}_{ij} \tag{34}$$

Symbols A, B, C in alphabetical order are considered to refer to ion species for which the selectivity decreases, relative to any given component, with A held by the exchanger the most strongly of all. A second index n (= 1,2,3) will indicate the plateau under consideration (for a column-concentration profile from upstream to downstream: plateau 1 is the feed plateau closest to the column inlet; plateau 3 is the presaturation plateau closest to the column outlet; plateau 2 is the intermediate plateau).

For the most general case, the starting point is in the interior of the composition diagram (Figure 4a), with coordinates for the i-th plateau x_{An}, x_{Bn}, x_{Cn} (each $\neq 0$). The corresponding equilibrium values y_{An}, y_{Bn}, y_{Cn} are calculated first. One then obtains two values of T from the expression:

$$T = \left[b \pm (b^2 - 4ac)^{0.5}\right] / 2a \qquad (35)$$

where

$$a_n = (\nu_A y_{An} + \nu_B y_{Bn} + \nu_C y_{Cn})$$

$$b_n = (\nu_B x_{Bn} + \nu_C x_{Cn}) x_{An} y_{Bn} y_{Cn} + (\nu_A x_{An} + \nu_C x_{Cn}) x_{Bn} y_{An} y_{Cn} + (\nu_A x_{An} + \nu_B x_{Bn}) x_{Cn} y_{An} y_{Bn}$$

$$c_n = (\nu_A x_{An} + \nu_B x_{Bn} + \nu_C x_{Cn}) y_{An} y_{Bn} y_{Cn}$$

The infinitesimal element of a composition path in the vicinity of the point under consideration is given by the ratio of the changes of the concentrations of two of the species, as:

$$\frac{dx_j}{dx_k} = \frac{dy_j}{dy_k} = \frac{\nu_j}{\nu_k} \frac{x_j y_j}{x_k y_k} \frac{Tx_k - y_k}{Tx_j - y_j} \tag{36}$$

The "root rule" discussed above gives the criterion to select the correct value for T from Equation 35; with the transitions numbered from upstream to downstream, the larger root of T calculated from feed plateau compositions will correspond to a 1,2 transition (adjacent to the feed composition); the smaller root of T calculated from the presaturation plateau compositions will correspond to a 2,3 transition (adjacent to the pre-existing solid compositions).

To calculate the exact composition path on the triangular diagram, it is necessary to follow a finite-difference method which requires the use of a high-speed computer. Exact and approximate methods are outlined by Klein, et al. (6), and by Vermeulen, Klein, and Hiester (8), together with some numerical examples (6).

In the present study, an attempt is made to calculate T values of the end plateaus by Equation 35 (variable-separation-factor method), and the intermediate plateau compositions are computed as intersections of the end-plateau path slopes. This can be justified for the softening process of sea water by ion exchange (and relative regeneration of the resin bed) by examining the relative locations of the points P_1 (corresponding to the feed-plateau composition) and P_3 (corresponding to the presaturation-plateau composition)

on the composition grid, as discussed below. Points P_1 and P_3 are shown in Figure 4 (b,c,d) for the same feed-plateau composition and for three different compositions of the solid-phase uniformly presaturated with: sodium chloride solution (Figure 4b); brine containing no calcium (Figure 4c); and brine containing all three components (Figure 4d).

It is evident from the figures that the exact composition path will not greatly differ from a straight line leaving P_1 or P_3, due to the limited range of composition changes. The values for the slopes of these straight lines are obtained by substituting the $T_{1,2}$ value, known from Equation 35 for the point at which the path leaves the feed plateau, into Equation 36 with feed-plateau conditions. This yields the slope $C_1 = (dx_i/dx_k)$ for the 1,2 transition. Similarly, the T value where the 2,3 path leaves the presaturation plateau leads, by Equation 36, to the slope $C_3 = (dx_i/dx_k)$ for the 2,3 transition. The paths intersect in the plateau-2 composition:

$$x_{k2} = \frac{C_1 x_{k1} - C_3 x_{k3} + x_{i3} - x_{i1}}{C_1 - C_3} \qquad (37)$$

with

$$x_{i2} = x_{i1} + C_1(x_{k2} - x_{k1}) \qquad (38)$$

The plateau y's are the equilibrium values given by the solutions of Equation 20.

From the intermediate-plateau composition it is

possible to calculate two more T values from Equation 35. The larger value corresponds to the end of the 1,2 transition, and the smaller value to the start of the 2,3 transition.

When the point representing either the presaturation plateau or the feed plateau is not in the interior of the composition diagram, the T values are determined as follows:

a. On a border of the composition diagram with $x_i = 0$ and $y_i = 0$ (see Figure 4b), one T value is given relative to a second component j (6):

$$T = \left[K_{ij}(y_j/x_j)^{\nu_i}\right]^{1/\nu_j} \tag{39}$$

The other T value, based on components j and k only, is

$$T = \frac{y_j y_k}{x_j x_k} \; \frac{\nu_j x_j + \nu_k x_k}{\nu_j y_j + \nu_k y_k} \tag{40}$$

which is Equation 36 explicit in T.

b. In a corner of the composition diagram with $x_i = 1$ and $y_i = 1$, the two T values are given by:

$$T = \left[\lim_{\substack{x_j \to 0 \\ y_j \to 0}} \left(\frac{y_j}{x_j}\right)\right]_{\substack{x_k = 0 \\ y_k = 0}}$$

$$T = \left[\lim_{\substack{x_k \to 0 \\ y_k \to 0}} \left(\frac{y_j}{x_j}\right)\right]_{\substack{x_j = 0 \\ y_j = 0}} \tag{41}$$

For $x_k = 0$, $y_k = 0$, the system becomes binary. In the mass-action case, Equation 20 applies (8) and is

$$\frac{y_j}{x_j} = \left(\frac{1 - y_j}{1 - x_j}\right)^{\nu_j/\nu_i} \left(\underset{\sim}{K}_{ij}\right)^{1/\nu_i} \tag{42}$$

Thus, the limit for $x_j \to 0$, $y_j \to 0$ is

$$T = \left(\underset{\sim}{K}_{ji}\right)^{1/\nu_i} \tag{43}$$

Similarly, the other T value is given by

$$T = \left(\underset{\sim}{K}_{kj}\right)^{1/\nu_i} \tag{44}$$

When all the T values relative to each transition and the intermediate plateau compositions are known, it is necessary to test each transition to determine whether it is abrupt or gradual. Several qualitative and quantitative rules have been given (6). Representative composition paths are shown in Figure 5. The arrows show the directions of decreasing values of T; a composition change in the direction of an arrow will correspond to a gradual transition. The route $P_1P_2P_3$ indicates the sequence of concentration that will occur in a column receiving a feed corresponding to P_1 and presaturated with a solution corresponding to P_3. The composition sequence P_1P_2 will occur in the upstream transition; the sequence P_2P_3 in the downstream transition. P_2, obtained as the intersection of the composition paths starting from P_1 and from P_3 [Figure 4 (b,c,d)], is the composition of the plateau zone intervening between transitions. In principle this result, as discussed above, does not apply exactly if either of the transitions is abrupt.

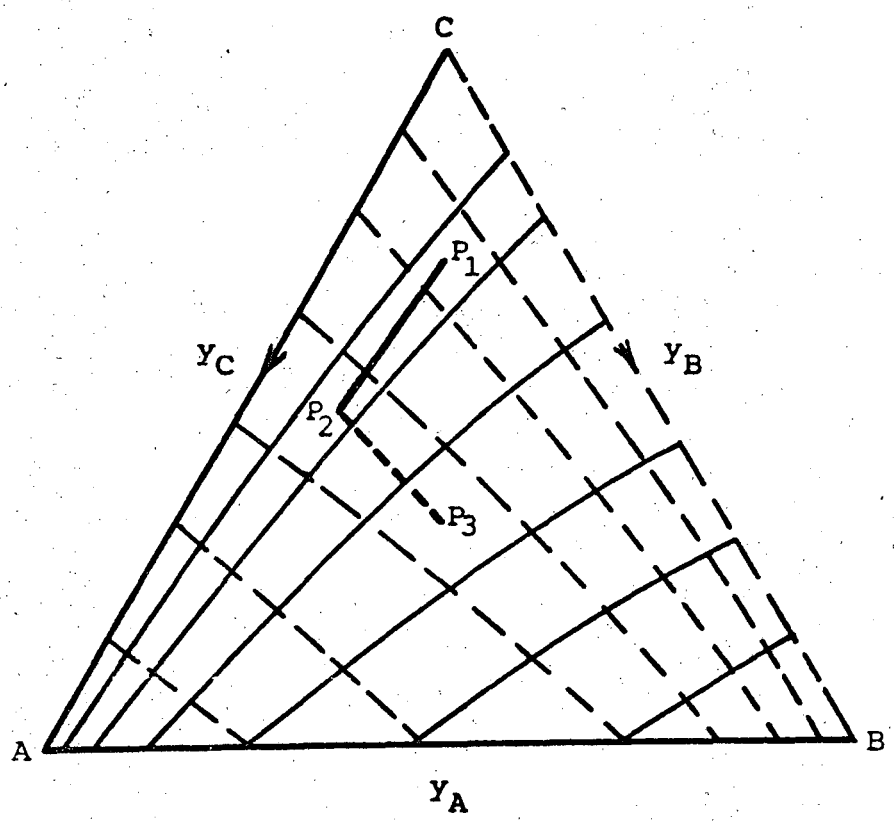

EXAMPLE OF COMPOSITION-PATH GRID.
SOLID LINES ARE 1,2 PATHS; DASHED LINES
ARE 2,3 PATHS

FIGURE 5

For any number of components, if the calculated T values along the path of a transition increase as the concentrations leave those of the earlier (downstream) plateau and approach those of the later (upstream) plateau, the calculated transition is real and hence gradual. If the T values increase in the reverse direction, the calculated transition is fictitious and hence abrupt (8).

Figure 6 shows a schematic designation of zone bounds for transitions and the resulting concentration-profile curve for a ternary system. Figure 7 gives the corresponding effluent-concentration history.

If a transition is gradual and if its equilibrium is described by constant separation factors, the local equilibrium X and Y values are identical for all components (calculated in relation to the two adjacent plateau compositions) and are given by the relations

$$X = \frac{R - \sqrt{R\bar{T}/T}}{R - 1} \tag{45}$$

and

$$Y = \frac{\sqrt{RT/\bar{T}} - 1}{R - 1} \tag{46}$$

where

$$x_i = x_i' + X(x_i'' - x_i'), \quad y_i = y_i' + Y(y_i'' - y_i'); \tag{47}$$

for the n-th transition

$$R_{n,n+1} = \left[\frac{T_{(n,n+1)''}}{T_{(n,n+1)'}}\right]^{1/2} \tag{48}$$

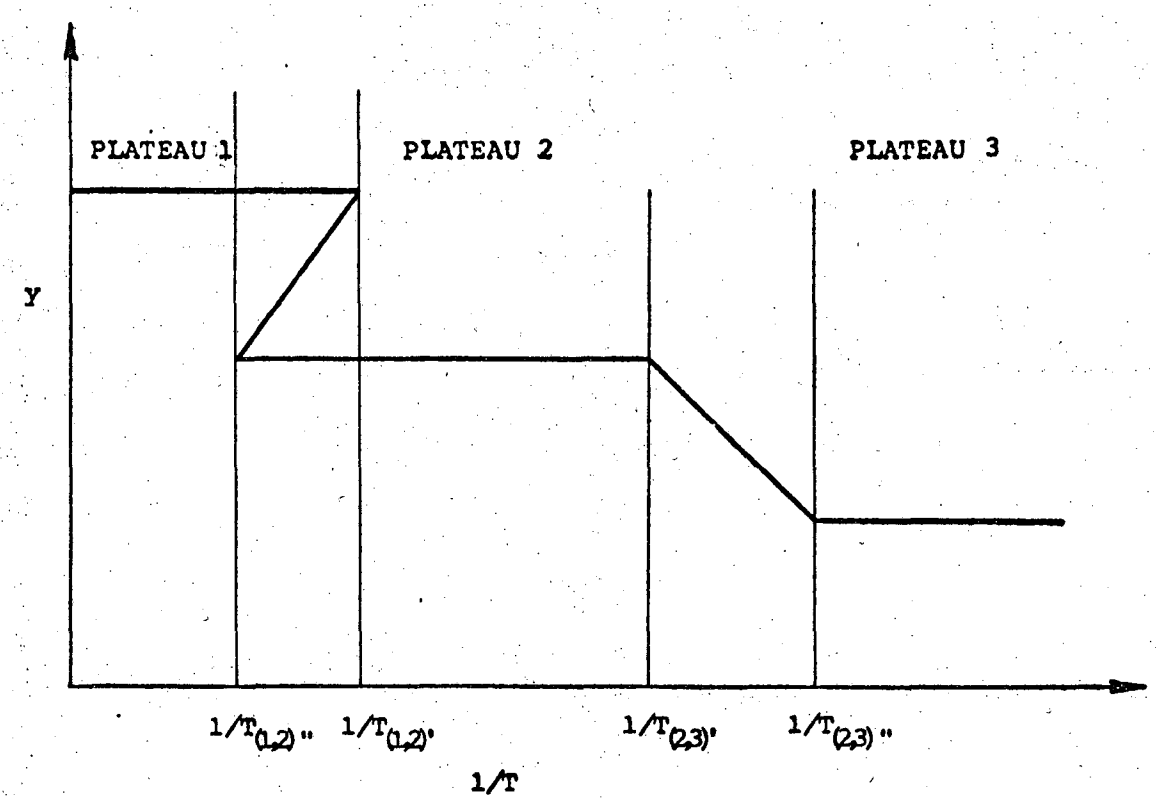

SCHEMATIC CONCENTRATION-PROFILE AND ZONE-BOUND DESIGNATIONS FOR ABRUPT TRANSITION 1,2 AND GRADUAL TRANSITION 2,3

FIGURE 6

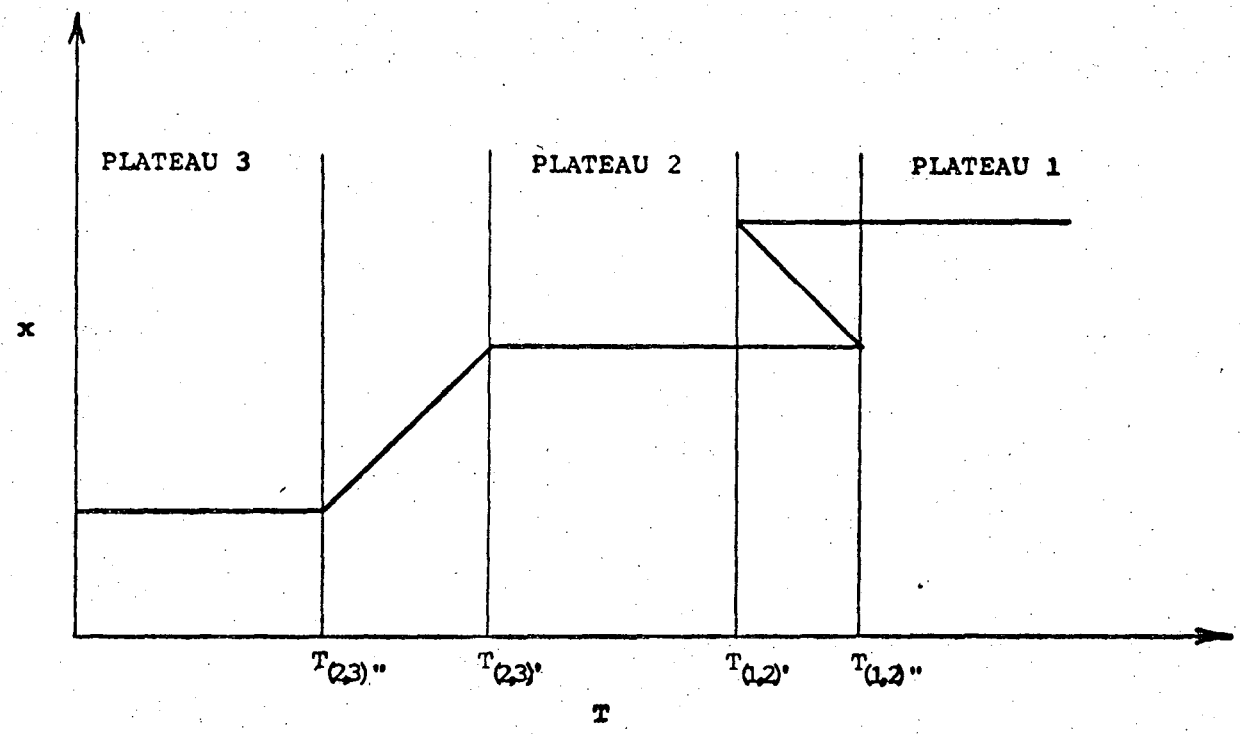

SCHEMATIC EFFLUENT-CONCENTRATION HISTORY AND ZONE-BOUND DESIGNATIONS FOR GRADUAL TRANSITION 2,3 AND ABRUPT TRANSITION 1,2

FIGURE 7

For a three-component system,

$$R_{1,2} = \left[\frac{T_{(1,2)''}}{T_{(1,2)'}}\right]^{1/2} \quad \text{and} \quad R_{2,3} = \left[\frac{T_{(2,3)''}}{T_{(2,3)'}}\right]^{1/2} \tag{49}$$

As $R < 1$ is the criterion for an abrupt transition, $T'' < T'$ becomes an alternate criterion as in binary separations.

10. Matching of Equilibrium-Theory Calculations to Experimental Runs

As stated in the Introduction, the equilibrium theory can be used to obtain quantitative boundary conditions for non-equilibrium systems. The stoichiometric average of the throughput parameter introduced by Equation 32 was derived by means of a global material balance, by Clazie (5). Equation 32 states that the stoichiometric average of the throughput parameter in a particular transition zone is determined by the concentrations in the adjacent plateau zones. Both in experimental runs (5,9) and in computer simulations (5,10) the plateau zones from the time of their first appearance are found empirically to occur exactly at the equilibrium-theory concentrations. Within the accuracy of this observation, for which no exceptions are known, the equilibrium value for $\bar{T}$ is identical to the non-equilibrium value. Thus the equilibrium theory can be used to calculate quantitative boundary conditions for either type of transition zone.

B. Rate Behavior

Deviations from local-equilibrium behavior must be accounted for by an effective rate of ion exchange, determined by one or more of the following diffusional steps:

1. Fluid-phase external mass-transfer
2. Fluid-phase pore diffusion
3. Reaction at the phase boundary
4. Solid-phase diffusion

Axial dispersion, a collective term that includes eddy dispersion and molecular diffusion, contributes negligibly to apparent mass-transfer resistance at the moderately high flow rates considered here. Mechanisms 1-2-3 and 1-3-4 each occur in series. For certain resins both mechanisms occur, in parallel, and the faster controls the rate. Steps 2 and 4 occur in parallel and are separated by Step 3, thus taking place in different phases. At different operating conditions, the same particle can show either solid- or pore-diffusion behavior, favoring the former if the pore fluid-concentration level is low and the latter if this level is high. This holds true when the pores subdivide the solid portion of an ion-exchange particle in a way that two interwoven networks of pore phase and solid phase provide alternative diffusion paths for the solute. "Openness" of the pore structure allows rapid exchange of material between the bulk fluid phase and the pores inside

the particle. It is evident that, if the pores are non-connected and the pore structure is "closed" (as Diamond-Shamrock Co.'s specifications for Duolite C-25 indicate), with an internal porosity as low as 6%, the fluid-phase inside the particle will not constitute a major alternative path of diffusion for the solute, even though the ratio D_p/D_f of solid-phase to fluid-phase diffusivity lies in the range of 10^{-2}.

1. Rate Equations

The system under consideration is truly a three-component system; in this section, however, it will be treated as a binary system. Because calcium breakthrough curves are of primary significance for the proposed process, only those curves are subjected to mass-transfer analysis; and because magnesium concentrations are small compared with sodium, the rates can be approximated by gross-ion/calcium counterdiffusion, where "gross ion" is predominately sodium. The rate equations here are expressed in terms of four dimensionless variables X, Y, R, and $\underset{\sim}{\Lambda}$, all previously defined.

a. Fluid-Phase External Mass Transfer. The rate of material transfer for the solute of interest is given by the classical relation involving the driving potential between the bulk fluid and the particle surface:

$$-\frac{dY}{dt} = \frac{k_f a_p}{\underset{\sim}{\Lambda}}(X - X^*) \qquad (50)$$

where k_f is the fluid-phase mass-transfer coefficient, a_p is the outer-surface interfacial area of the particles per unit volume of contacting system (solid plus fluid), and X^* is the dimensionless fluid-phase concentration in equilibrium with the outer surface of the solid. The following relation, empirically fitted to apply to liquid-solid contact (8), applies for aqueous solution and a bed void fraction of 0.40:

$$k_f a_p = \frac{2.62(D_f F/S)^{0.5}}{d_p^{1.5}} \tag{51}$$

where d_p is the particle diameter; S is the cross-sectional area of the column, and F/S is the superficial velocity. If external mass transfer only controls the ion-exchange rate in a fixed bed, a number of mass-transfer units N_f can be defined which will convert the rate equation to non-dimensional form. When the rate equation is expressed with dimensionless concentrations, the product $N_f T$ is a dimensionless time given by the product of an effective time $\hat{t}=\hat{V}/F$ and the rate coefficient. Thus,

$$N_f \underset{\sim}{T} = \frac{k_f a_p}{\underset{\sim}{\Lambda}} \frac{\hat{V}}{F} = \frac{k_f a_p}{\underset{\sim}{\Lambda}} \frac{V - v\epsilon}{F} \tag{52}$$

and the ion-exchange rate becomes

$$\left(\frac{\partial Y}{\partial N_f \underset{\sim}{T}}\right)_{N_f} = X - X^* \tag{53}$$

Also, N_f is obtained through division by $\underset{\sim}{T} = \hat{V}/\underset{\sim}{\Lambda}v$, which gives

$$N_f = \frac{k_f a_p}{\underset{\sim}{\Lambda}} \frac{v}{F} = k_f a_p \frac{hS}{F} \tag{54}$$

b. <u>Fluid-Phase Pore Diffusion</u>. The rigorous diffusion rate equation for fluid-phase transport through a network of fluid-filled pores inside the particles is often advantageously represented by a modified linear-driving-force approximation (14). The dimensionless ion-exchange rate is, in this case:

$$\left(\frac{\partial Y}{\partial N_{pore} \underset{\sim}{T}}\right)_{N_{pore}} = Y^* - Y \tag{55}$$

where Y^* is the dimensionless concentration of the solute that would be in equilibrium with the instantaneous fluid-phase concentration outside the particle; and N_{pore} is given by

$$N_{pore} = \psi_{pore} k_{pore} a_p \frac{hS}{F} \tag{56}$$

where

$$k_{pore} a_p = \frac{60 D_{pore}}{d_p^2}(1 - \epsilon) \tag{57}$$

with $\psi_{pore} = 0.775/(1 - 0.225R^{0.40})$. The term D_{pore} represents the diffusivity of the solute in the fluid phase inside the pores.

c. Reaction at the Phase-Boundary. The actual ion-exchange reaction occurring at solid-fluid interfaces usually is extremely rapid. However, even when the diffusion steps control the rate, it may still be convenient to describe a system by its apparent second-order kinetic behavior, which provides a good approximation to a more complex exact form. The dimensionless rate equation for this case is (8)

$$\left(\frac{\partial Y}{\partial N_R \underset{\sim}{T}}\right)_{N_R} = X(1 - Y) - RY(1 - X) \qquad (58)$$

where $N_R = \mathcal{K} \underset{\sim}{\Lambda} (hS/F)$.

d. Solid-Phase Diffusion. As in Step 2, the rigorous diffusion equation for diffusion in a spherical particle is approximated by a linear-driving-force relation. The dimensionless rate equation is

$$\left(\frac{\partial Y}{\partial N_p \underset{\sim}{T}}\right)_{N_p} = Y^* - Y \qquad (60)$$

and

$$N_p = \psi_p \underset{\sim}{\Lambda} k_p a_p \frac{hS}{F} \qquad (61)$$

where

$$k_p a_p = \frac{60 D_p}{d_p^2} \qquad (62)$$

with D_p the solid-phase diffusivity. The factor ψ_p is given approximately by $\psi_p = 0.894/(1 - 0.106R^{0.25})$ for $R < 1$; for $R > 1$, $\psi_p \sim 1$.

2. Combined Resistances

a. Fluid Side. External mass transfer and axial dispersion operate in series, so that the effective resistance (or cause of spreading) is the sum of the separate resistances.

$$1/N_{cf} = 1/N_{cd} = (1/N_f + 1/N_d) \tag{63}$$

Usually $1/N_d$ is negligible as compared with $1/N_f$ at the flow rates considered here.

b. Particle Side. When particle-phase and pore diffusion operate in parallel, the effective rate is the sum of these two rates. If particle diffusion predominates,

$$N_{cp} = N_p + \frac{N_{pore}}{\underset{\sim}{\Lambda}} \tag{64}$$

If pore diffusion,

$$N_{c,pore} = N_{pore} + \underset{\sim}{\Lambda} N_p \tag{65}$$

3. Overall Resistances

Except for the case of a linear isotherm ($R = 1$), when the solutions for all mechanisms are nearly identical, the sum of the resistances does not give directly the overall resistance. Correction terms (b's) are defined by the following relations, with subscript "o" indicating overall

number of transfer units:

$$\frac{1}{N_{cf}} + \frac{1}{N_{cp}} = \frac{b_f}{N_{of}}$$

$$= \frac{b_p}{N_{op}}$$

$$= \frac{b_R}{N_R} \qquad (66)$$

For all cases where one or more mass-transfer mechanisms control the rate, the subscript-free ratio N/b can be expressed as a function of the column length to particle-diameter ratio h/d_p, the Péclet number for flow $d_p(F/S)/D_f$, and a ratio of the controlling diffusivity to the fluid-phase diffusivity. Figure 8 gives numerical values of Nd_p/bh. If fluid-side spreading effects control, the effective N is given by the uppermost curve. If particle-side diffusivities control, the effective N is given by a point below the upper envelope, on the appropriate diffusional contour. Near the intersections of the diffusional contours with the outer envelope, N is the reciprocal of the sum of the reciprocals for the fluid-side and particle-side N's.

For R values between 0.6 and 1.6, $b_p = 1$ and $b_f = 1$ are the suggested values (8). The correction term for the reaction-kinetic rate is:

$$b_R = \frac{2b_p}{R + 1} = \frac{2}{R + 1} \qquad (67)$$

Since in all cases N and v are related by constants, the

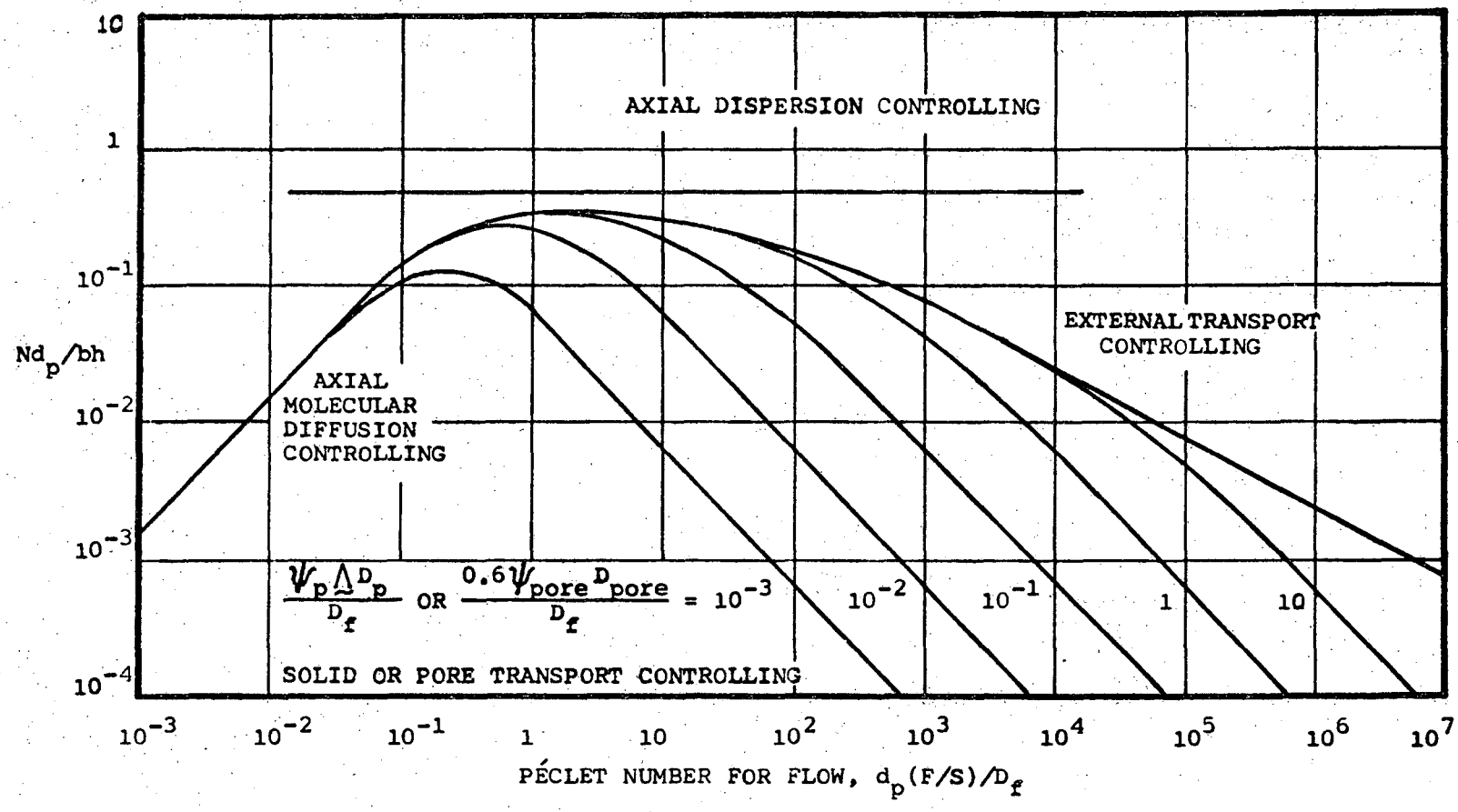

EFFECTS OF PÉCLET GROUP, PARTITION RATIO, AND DIFFUSIVITY RATIO ON HEIGHT OF A REACTION UNIT

FIGURE 8

material-balance relation of Equation 32, first transformed to,

$$-\left(\frac{\partial x_i}{\partial v}\right)_{Tv} = \left(\frac{\partial y_i}{\partial Tv}\right)_v \tag{68}$$

becomes, in dimensionless form,

$$-\left(\frac{\partial X}{\partial N}\right)_{N\underset{\sim}{T}} = \left(\frac{\partial Y}{\partial N\underset{\sim}{T}}\right)_N = \left[\text{dimensionless driving force}\right] \tag{69}$$

with N carrying the appropriate subscript designation. Solution of any dimensionless rate equations with Equation 69 gives X and Y as functions of N and $\underset{\sim}{T}$, as well as of R.

Sets of limited results in particular regions of equilibrium behavior, for specific algebraic models of equilibrium and of rate-determining mechanisms, are available and are discussed in (8), but they do not constitute a general analytical solution to the partial differential equations above.

4. <u>General Nonlinear-Equilibrium Reaction-Kinetic Result</u>

The reaction-kinetic treatment at constant R for non-linear equilibrium, with non-linear addition of resistance using the appropriate value of b, will be adopted here. This method is preferable to others for favorable equilibrium ($0.6 < R < 1$) and is moderately accurate for unfavorable equilibrium ($R > 1$), for any value of the number of reaction units. The most general relation for breakthrough behavior has been developed by Thomas (15), which includes the equilibrium parameter R as an independent variable along

with N_R and the throughput parameter $\underset{\sim}{T}$.

With the dimensionless-driving force given by Equation 58, the material balance (Equation 69) becomes:

$$-\left(\frac{\partial X}{\partial N_R}\right)_{N_R T} = \left(\frac{\partial Y}{\partial N_R \underset{\sim}{T}}\right)_{N_R} = X(1 - Y) - RX(1 - X) \qquad (70)$$

Numerical values of the solutions of Equation 70 have been computed and tabulated by Opler and Hiester (16). More extensive tables by Vermeulen, Nassiri, Nellis, and LeMaguer (17) are now available. For intermediate values of R and N_R, cross-plots covering the working range of R values that apply in design calculations are given in (8), with $1-\underset{\sim}{T}$ (or $\underset{\sim}{T}-1$) as function of R, at various values of N_R, for five constant values of X. A typical cross-plot for X = 0.9 is shown in Figure 9. Experimental breakthrough data can be used to obtain N_R values (or, alternatively, rate values) once the equilibrium parameter is known. In this event, the experimental data and the theoretical solutions $X = f(\underset{\sim}{T}, N_R, R)$, for various values of N_R, and at the applicable equilibrium parameter R, can be plotted together on a probability ordinate for X versus a linear abscissa for $\underset{\sim}{T}$; the theoretical curve matching the experimental plot will give the number of reaction units N_R. This method is useful in general; however, if the slope of the breakthrough curve at X = 0.5 can be calculated for the transition under consideration, the number of reaction units can be

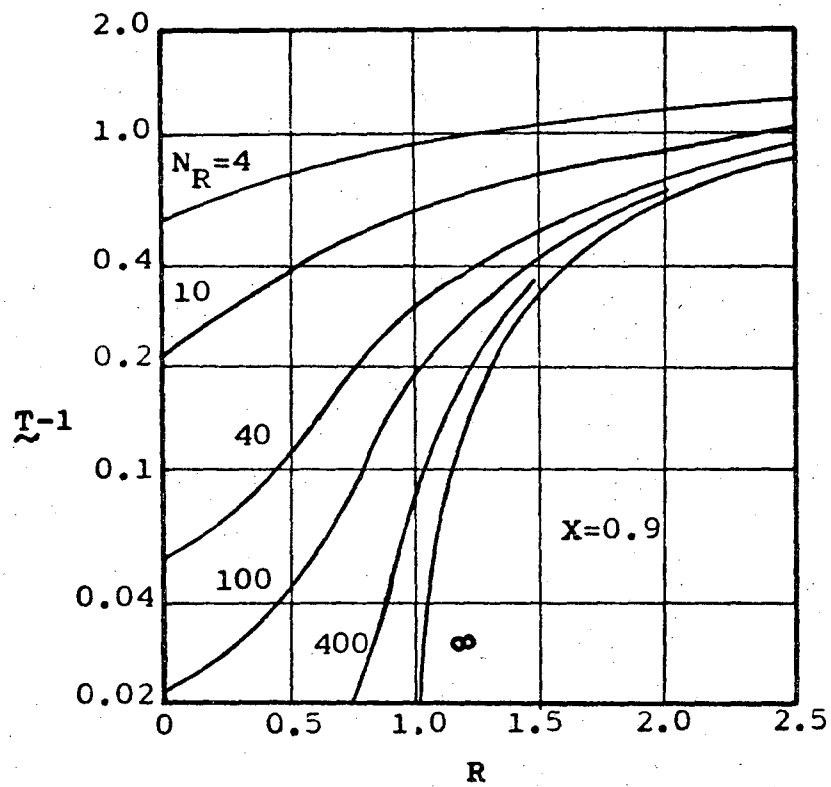

CROSS-PLOT OF THROUGHPUT RATIO AT X = 0.90
AGAINST EQUILIBRIUM PARAMETER

FIGURE 9

determined from this midpoint slope, as suggested by Thomas (15) and Gilliland and Baddour (18). Values of the midpoint slope versus the number of reaction units N_R at various values of the equilibrium parameter R are shown in Figure 10.

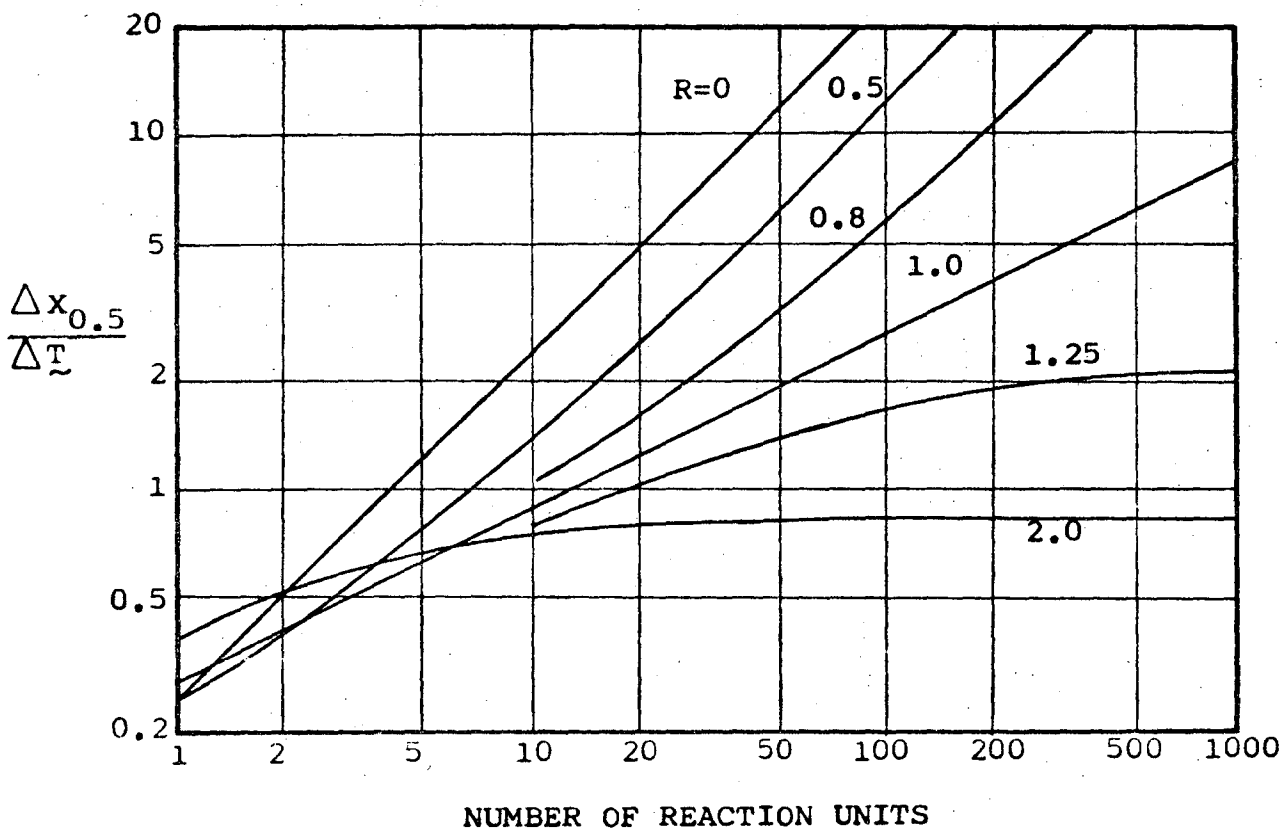

DIMENSIONLESS MIDPOINT SLOPE AS A FUNCTION OF EQUILIBRIUM PARAMETER AND OF NUMBER OF REACTION UNITS

FIGURE 10

III. APPLICATION

The criteria for determining both the equilibrium and the rate behavior of ion-exchange columns, outlined in the Theory section, are now applied to experimental results obtained from sea-water softening and saturated-resin regeneration runs. Operating conditions for the runs that were analyzed are given in Table I.

A. Equilibrium Behavior

1. Resin Capacity and Selectivity. The sea-water softening process under consideration uses a macroporous sulfonated-polystyrene ion-exchange resin, Duolite C-25*, having a uniform bead structure with 5 to 15% internal porosity (a value around 6% has been indicated to us by the manufacturer).

A range of values for the total dry exchange capacity of the resin with 5 to 6% divinylbenzene crosslinking is reported in the literature (2,8,11). Klein, Villena-Blanco, and Vermeulen, in their determination of ion-exchange equilibrium data (2), indicate the exchange capacity Q to be 4.85 meq/gm. Abrams and Benezra (11) in a classification of several ion-exchange resins, report that Q ranges between 5.10 meq/gm and 5.30 meq/gm.

---

*Manufactured by Diamond-Shamrock Corporation, Western Division, Redwood City, California.

TABLE I

OPERATING CONDITIONS FOR EXPERIMENTAL RUNS

a. SATURATION RUNS

RUN	2S	3S	4S	21S
Flow Rate, gal/(ft^2 min)	8.0	5.0	4.0	3.0
Total Normality, eq/l	0.6166	0.6166	0.6158	0.6142
Calcium Normality, eq/l	0.0207	0.0207	0.0205	0.0206
Magnesium Normality, eq/l	0.1080	0.1080	0.1082	0.1086

b. REGENERATION RUNS
Concentration factor n = 2; pure NaCl solution

RUN	1RA	5R	9R
Flow Rate, gal/(ft^2 min)	1.0	2.84	4.10
Total Normality, eq/l	1.24	1.24	1.267

c. REGENERATION RUNS
Concentration factor n = 4

RUN	1R	2R	3R
Flow Rate, gal/(ft^2 min)	4.0	2.0	0.5
Total Normality, eq/l	2.488	2.457	2.4455
Calcium Normality, eq/l	0.000	0.0044	0.00408
Magnesium Normality, eq/l	0.305	0.2955	0.2954

The total capacity of this type of resin can be calculated theoretically, as shown by Helfferich (1), by noting that monosulfonated styrene-divinylbenzene copolymers in H^+ form consist predominantly of units

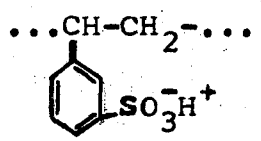

Each unit $C_3H_8O_3S$ has the formula weight 184.2 and carries one fixed ionic group. The resin contains also sulfonated divinylbenzene and ethylstyrene units (of formula weights 210.2 and 212.2, respectively) in about equal proportions. Thus, a resin with 5.5% divinylbenzene crosslinking probably contains also 5.5% of ethylstyrene. The total exchange capacity then has the value

$$Q = 1000(0.89/184.2 + 0.055/210.2 + 0.055/212.2) = 5.35 \text{ meq/gm}$$

Values of $K_{DM}Q$, where K_{DM} is the selectivity coefficient defined by Equation 2, are used to characterize the equilibrium between solid and fluid phase. Klein, Villena-Blanco, and Vermeulen (2) report the result of a single determination on Duolite C-25 at 20°C, a total solution normality $C_o = 0.62$ N, and $x_A = 0.1$, $x_C = 0.9$, to be $K_{AC}Q = 4.70$ meq/ml. From their exchange-capacity and $K_{AC}Q$ value, the selectivity coefficient becomes

$$K_{AC} = \frac{K_{AC}Q}{Q} = \frac{4.70}{4.85} = 0.97 \text{ gm/ml}$$

Assuming K_{AC} to be a constant, the theoretical value of Q leads to

$$(K_{AC}Q)_{theor} = 0.97x5.35 = 5.19 \text{ meq/ml}$$

Averaging between this value and 4.70, in turn, gives

$$(K_{AC}Q)_{av} = 4.95 \cong 5.00 \text{ meq/ml}$$

which corresponds to a Q of 5.10 meq/gm.

For magnesium-sodium equilibrium on Duolite C-25, the same authors report the single-determination result, at the above-listed operating conditions:

$$K_{BC}Q = 2.30 \text{ meq/ml}$$

With the Q value of 4.85 meq/gm, the value of K_{BC} would be 0.47 gm/ml. Experiments in columns suggest that this K value is high, and that a value of 0.45 is more likely. With the average Q of 5.10 meq/gm, the best working value becomes

$$(K_{BC}Q)_{av} \cong 2.3 \text{ meq/ml}$$

In the analysis that follows, the estimated times (or volumes) of arrival of the fluid front and of the transitions do not yield exact material balances with the experimental

concentration histories. In each run, this discrepancy will be allotted to the experimental $Q\rho_b v$ product, so that the T scale originally assigned to the experimental time (or volume) scale will be adjusted to match the theoretical fluid front and the theoretical material balance. The assumption underlying this adjustment is that K's and Q are constant throughout, and that $v\rho_b$ or C_o is changing. The correction is under 3% in all cases; other methods of adjustment, based for instance on Donnan uptake, would give essentially the same numerical conclusions as this method.

2. Equilibrium-Theory Predictions. Use of mass-action equilibrium relationships established for the three-component system under consideration, with the chosen calcium-sodium and magnesium-sodium selectivity coefficients and known boundary conditions (feed and presaturation composition), gives the equilibrium composition of the feed and presaturation plateaus in the solid and fluid phases. With these results, the equilibrium-theory equations developed earlier (the form of which depends on the boundary conditions) permit calculation of throughput-parameter values for the transition extremes; intermediate-plateau compositions; stoichiometric averages of throughput parameter; and the equilibrium-parameter values for each transition. The theoretical effluent-concentration histories for calcium and magnesium derived from this information are compared to experimental effluent-concentration-history

results. These results were obtained at the Sea Water Conversion Laboratory, where several saturation and regeneration runs were carried out in a laboratory column having a nominal length of four feet, filled with Duolite C-25 of 16-50 mesh size, and operated downflow for saturation and upflow for regeneration.

a. Saturation Runs. The effluent-concentration histories of calcium and magnesium for Runs 4S and 21S are shown in Figures 11 and 12, respectively. For Run 4S, where the resin, before the softening step is started, is saturated with regenerant brine (four times as concentrated as sea water and containing sodium in a higher and calcium in a lower proportion), the effluent concentration of both calcium and magnesium first decreases, approaching the values of equilibrium with the presaturated-resin concentrations, as the exhausted regenerant brine occupying the bed void space is displaced by incoming sea water; thereafter, removal of sodium from the resin begins, with magnesium building up its concentration in the effluent and in the resin, and with calcium (more tightly held by the resin) remaining at practically its minimum level, while the magnesium concentration reaches a maximum. Subsequently the calcium effluent concentration rises, and the magnesium and sodium concentrations decrease to their feed-concentration levels.

Presaturation for Run 21S was carried out with pure NaCl solution of twice the sea-water normality; therefore,

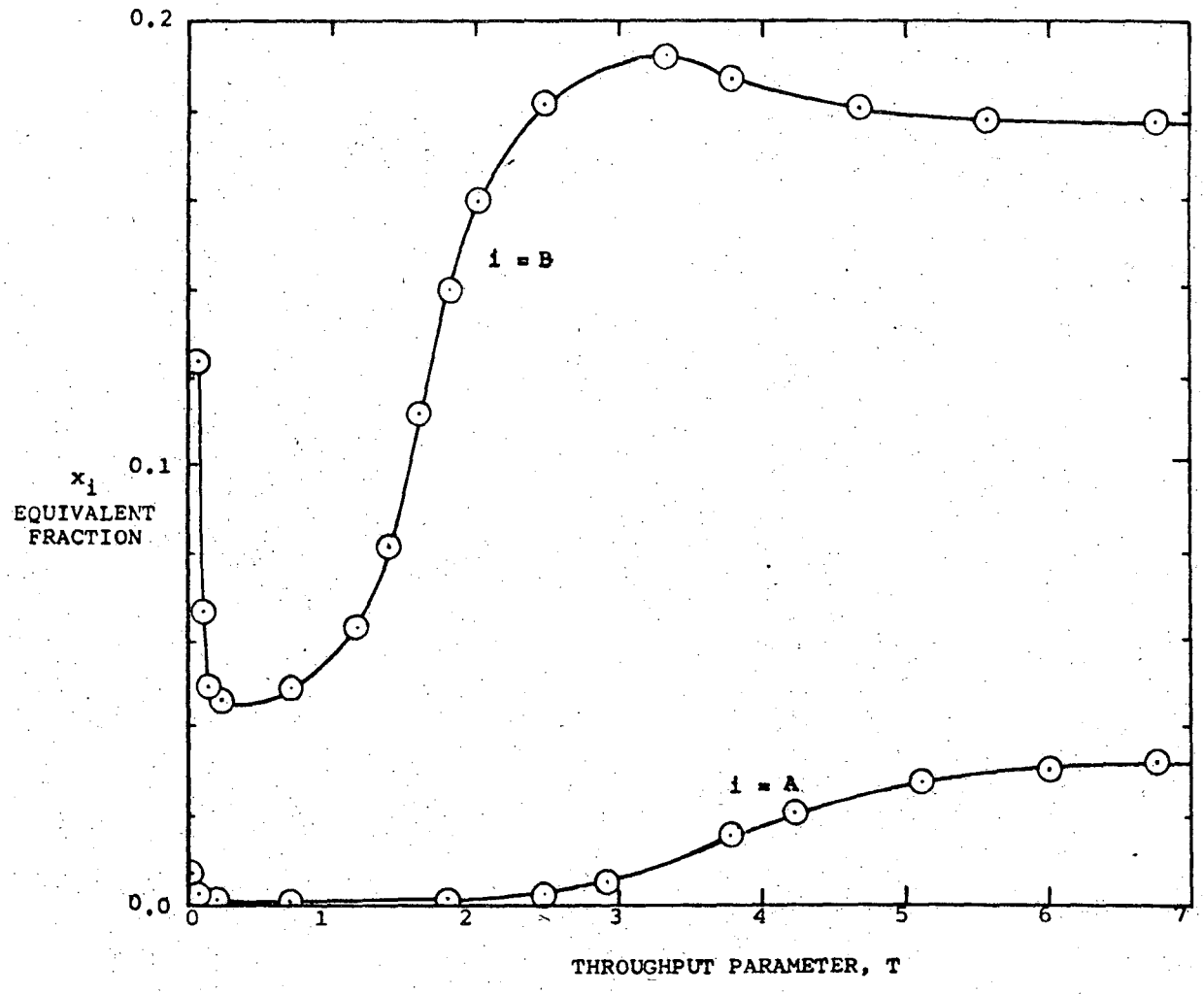

SEA-WATER SOFTENING BY A COLUMN UNIFORMLY PRESATURATED WITH CALCIUM, MAGNESIUM, AND SODIUM IONS: CALCIUM AND MAGNESIUM EFFLUENT-CONCENTRATION HISTORIES FOR RUN 4S

FIGURE 11

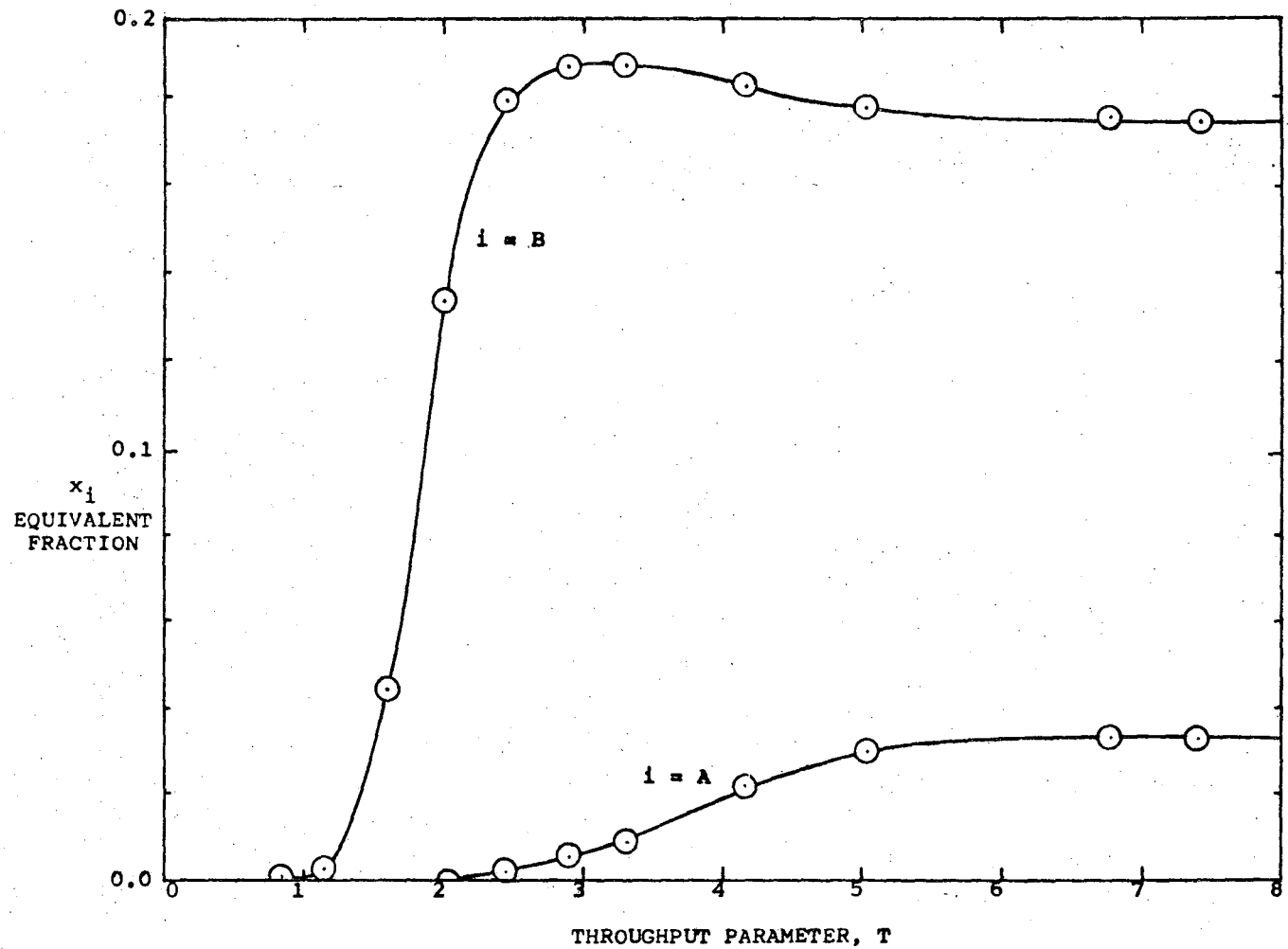

SEA-WATER SOFTENING BY COLUMN INITIALLY IN SODIUM FORM: CALCIUM AND MAGNESIUM EFFLUENT-CONCENTRATION HISTORIES FOR RUN 21S

FIGURE 12

the concentrations of both magnesium and calcium, in the effluent in equilibrium with resin containing neither of these ions, start from zero. As shown in Figure 12, the subsequent behavior of concentration histories is similar to the behavior described for Run 4S. For all the softening runs analyzed, Table II-a gives the theoretical plateau-zone solid- and fluid-phase compositions. Table III-a gives, in succession, throughput parameter values (T')'s and (T")'s, determining the extremes of each transition; stoichiometric averages $\overline{T}_{1,2}$ and $\overline{T}_{2,3}$ of throughput parameter, calculated by Equation 32 from the known adjacent-plateau solid- and fluid-phase compositions; and the equilibrium-parameter values $R_{1,2}$ and $R_{2,3}$, calculated by Equations 49, from the known (T')'s and (T")'s. Figures 13 and 14 show the experimental calcium and magnesium effluent concentration histories for Runs 4S and 21S, together with the calculated equilibrium-theory histories derivable from Tables II-a and III-a. All transitions involved in saturation runs are characterized by an equilibrium parameter less than unity, hence the theoretical curves are abrupt.

It is of interest to compare the theoretical concentration levels with the identifiable constant-composition zones for the calcium and magnesium experimental effluent histories, particularly for the third (presaturation) and second (intermediate) plateaus the first (feed) plateau, furthest upstream,

TABLE II-a

CALCULATED PLATEAU-ZONE COMPOSITIONS FOR SATURATION RUNS

RUN	2S	3S	4S	21S
Feed Plateau				
x_{A1}	0.0336	0.0336	0.0333	0.03354
x_{B1}	0.175	0.175	0.1760	0.1770
y_{A1}	0.1320	0.1320	0.1310	0.1318
y_{B1}	0.3169	0.3169	0.3185	0.3198
Intermediate Plateau				
x_{A2}	0.00109	0.00104	0.0015	0.000
x_{B2}	0.1965	0.1965	0.1969	0.198
y_{A2}	0.0049	0.0046	0.0066	0.000
y_{B2}	0.4014	0.4015	0.4013	0.409
Presaturation Plateau				
x_{A3}	0.00054	0.00051	0.00073	0.000
x_{B3}	0.0363	0.0367	0.0365	0.000
y_{A3}	0.0037	0.00345	0.00497	0.000
y_{B3}	0.1138	0.1147	0.1142	0.000

TABLE II-b

CALCULATED PLATEAU-ZONE COMPOSITIONS FOR REGENERATION RUNS
(n = 2)

RUN	1RA	5R	9R
Feed Plateau			
x_{C1}	1.000	1.000	1.000
y_{C1}	1.000	1.000	1.000
Intermediate Plateau			
x_{A2}	0.0321	0.0336	0.0373
x_{B2}	0.0000	0.0000	0.0000
y_{A2}	0.1095	0.1110	0.1142
y_{B2}	0.0000	0.0000	0.0000
Presaturation Plateau			
x_{A3}	0.0510	0.0513	0.0531
x_{B3}	0.2690	0.2650	0.3690
y_{A3}	0.1324	0.1335	0.1362
y_{B3}	0.3210	0.3172	0.3170

TABLE II-c

CALCULATED PLATEAU-ZONE COMPOSITIONS FOR REGENERATION RUNS
(n = 4)

RUN	1R	2R	3R
Feed Plateau			
x_{A1}	0.0000	0.0018	0.0017
x_{B1}	0.1226	0.1203	0.1208
y_{A1}	0.0000	0.0037	0.0035
y_{B1}	0.1152	0.1138	0.1147
Intermediate Plateau			
x_{A2}	0.0761	0.0744	0.0740
x_{B2}	0.1077	0.1064	0.1067
y_{A2}	0.1373	0.1356	0.1354
y_{B2}	0.0893	0.0892	0.0897
Presaturation Plateau			
x_{A3}	0.0701	0.0692	0.0690
x_{B3}	0.3660	0.3614	0.3610
y_{A3}	0.1330	0.1321	0.1321
y_{B3}	0.3192	0.3170	0.3170

TABLE III-a

THROUGHPUT-PARAMETER VALUES FOR SATURATION RUNS

RUN	2S	3S	4S	21S
$T_{(1,2)'}$	3.4765	3.4760	3.4810	3.4746
$T_{(1,2)''}$	4.4223	4.3810	4.4030	4.4200
$T_{(2,3)'}$	1.2930	1.2966	1.2890	1.2940
$T_{(2,3)''}$	2.6768	2.6748	2.6812	3.7450
$\bar{T}_{1,2} = \Delta y_i / \Delta x_i$	3.9360	3.9360	3.9265	3.9284
$\bar{T}_{2,3} = \Delta y_i / \Delta x_i$	1.7956	1.7943	1.7895	2.0660
$R_{1,2}$	0.887	0.890	0.889	0.920
$R_{2,3}$	0.695	0.696	0.693	0.791

TABLE III-b

THROUGHPUT-PARAMETER VALUES FOR REGENERATION RUNS
(n = 2)

RUN	1RA	5R	9R
$T_{(1,2)'}$	4.032	4.030	3.946
$T_{(1,2)''}$	2.9195	2.827	2.623
$T_{(2,3)'}$	1.570	1.570	1.537
$T_{(2,3)''}$	0.978	0.980	0.9744
$\bar{T}_{1,2} = \Delta y_i / \Delta x_i$	3.410	3.300	3.070
$\bar{T}_{2,3} = \Delta y_i / \Delta x_i$	1.195	1.197	1.180
$R_{1,2}$	1.175	1.190	1.230
$R_{2,3}$	1.265	1.266	1.256

TABLE III-c

THROUGHPUT-PARAMETER VALUES FOR REGENERATION RUNS
(n = 4)

RUN	1R	2R	3R
$T_{(1,2)'}$	2.04	2.05	2.06
$T_{(1,2)''}$	1.608	1.625	1.63
$T_{(2,3)'}$	0.8513	0.858	0.860
$T_{(2,3)''}$	0.9250	0.9252	0.9250
$\bar{T}_{1,2} = \Delta y_i / \Delta x_i$	1.804	1.820	1.830
$\bar{T}_{2,3} = \Delta y_i / \Delta x_i$	0.890	0.893	0.895
$R_{1,2}$	1.13	1.123	1.124
$R_{2,3}$	0.960	0.963	0.964

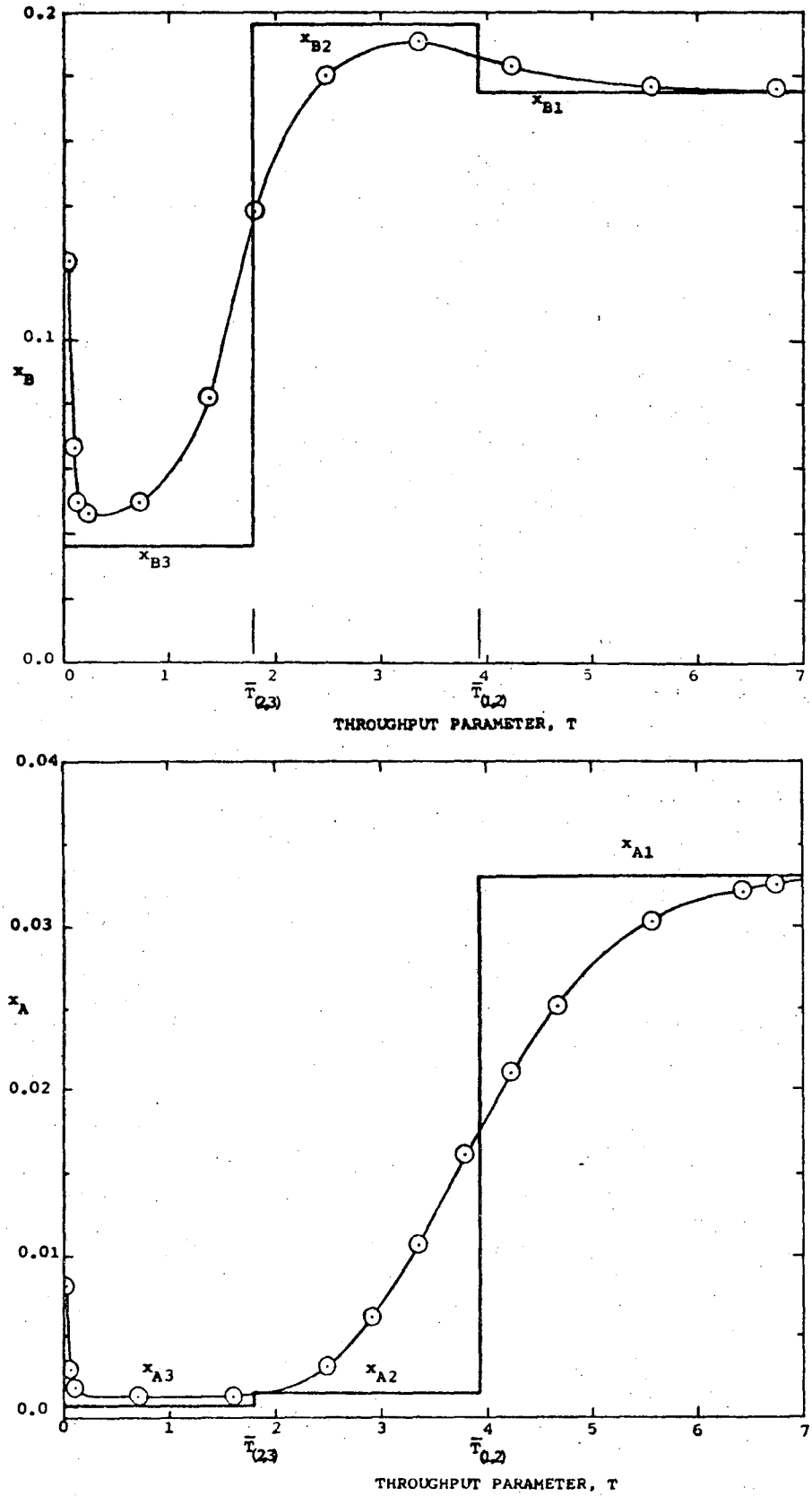

PREDICTED PLATEAUS AND TRANSITIONS COMPARED TO EXPERIMENTAL CALCIUM AND MAGNESIUM EFFLUENT-CONCENTRATION HISTORIES FOR RUN 4S; REGENERATION BY FOUR TIMES CONCENTRATED BRINE

FIGURE 13

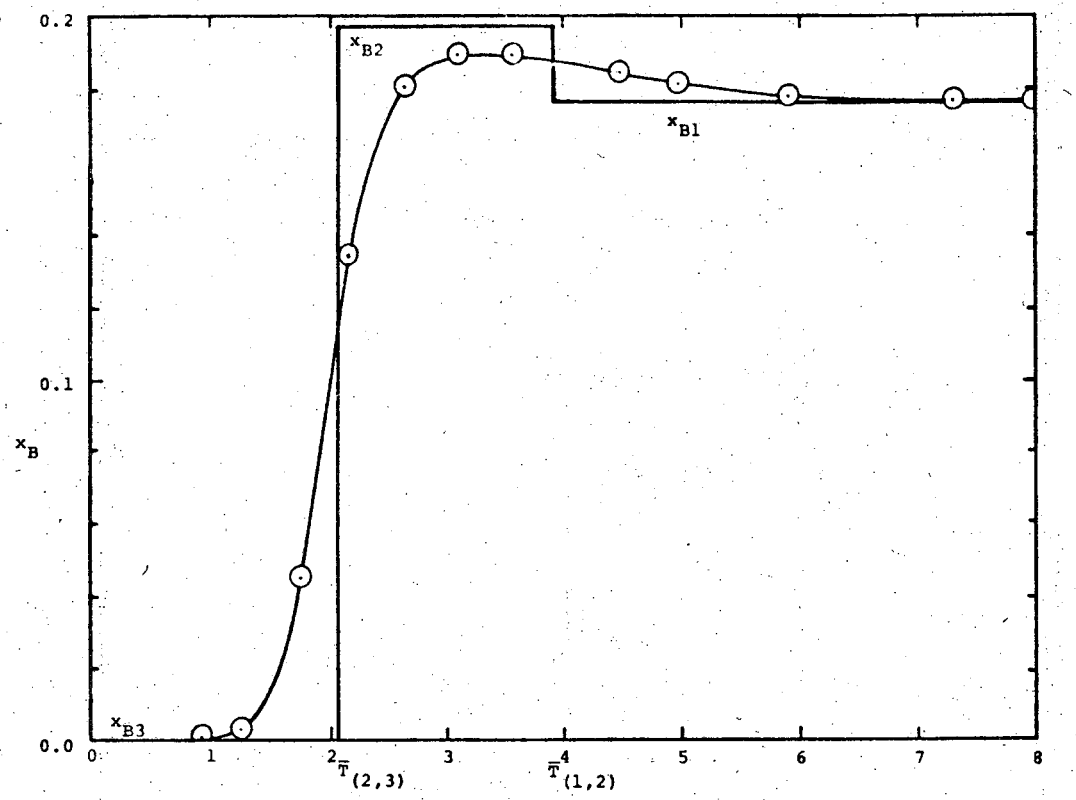

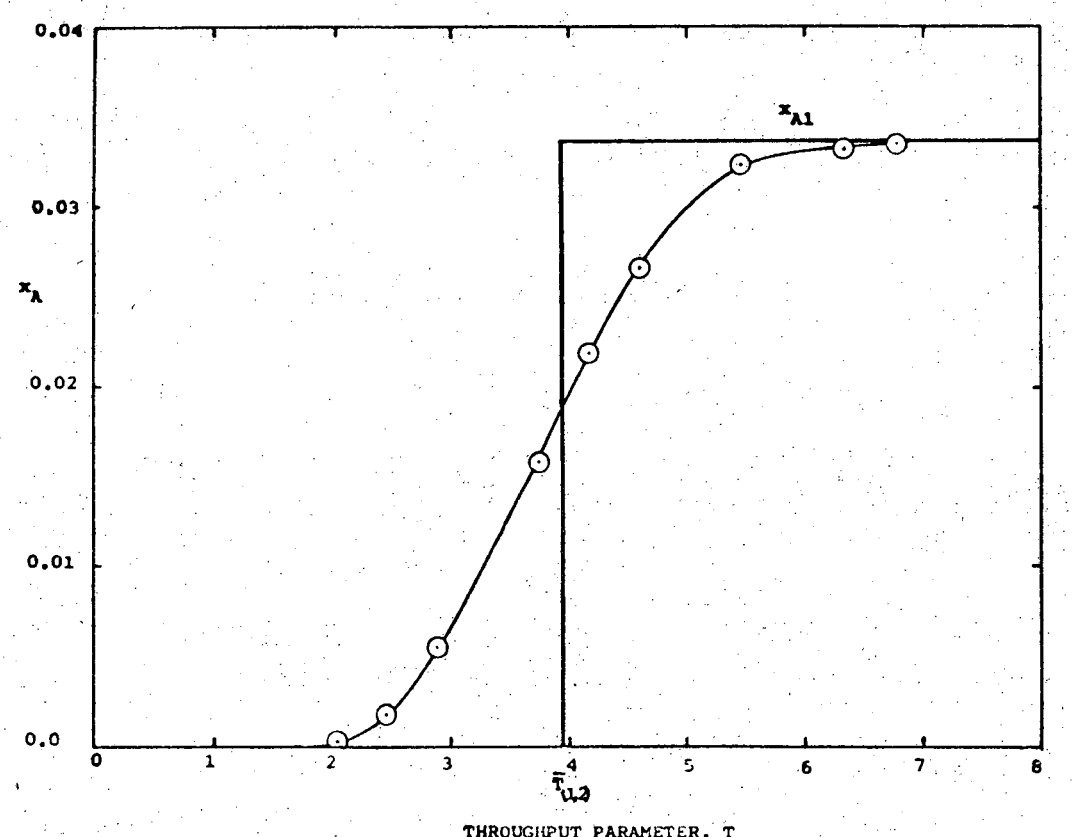

PREDICTED PLATEAUS AND TRANSITIONS COMPARED TO EXPERIMENTAL CALCIUM AND MAGNESIUM EFFLUENT-CONCENTRATION HISTORIES FOR RUN 21S; COLUMN INITIALLY IN SODIUM FORM

FIGURE 14

provides no comparison because the effluent merely matches the column input . For Run 4S, calcium and magnesium concentrations do not reach the predicted concentration levels in the presaturation and intermediate plateau zones (Figure 13). Figure 14, representing Run 21S, shows that agreement is good between the theoretical and experimental concentrations for magnesium on the presaturation plateau (where calcium is absent), and for calcium on the intermediate-plateau zone; in this region, magnesium concentration does not reach the predicted level. Mass-transfer resistances cause contiguous transitions to overlap: here rate behavior predominates over the predicted equilibrium behavior. A more thorough discussion is given below in relation to the kinetic analysis of the experimental runs.

b. Regeneration Runs (n = 2). Tables II-b and III-b give the equilibrium theory results for these runs. Figure 15 shows the effluent-concentration histories for calcium and magnesium in the case of Run 1RA.

A void-saving technique was adopted in which spent regenerant brine of high calcium and magnesium content saved from the previous regeneration was used to wash away unsoftened sea water still present in the bed void spaces, before fresh concentrated brine was passed through the bed. Displacement of sea water by the spent regenerant results in an inert fluid breakthrough without exchange of ions between

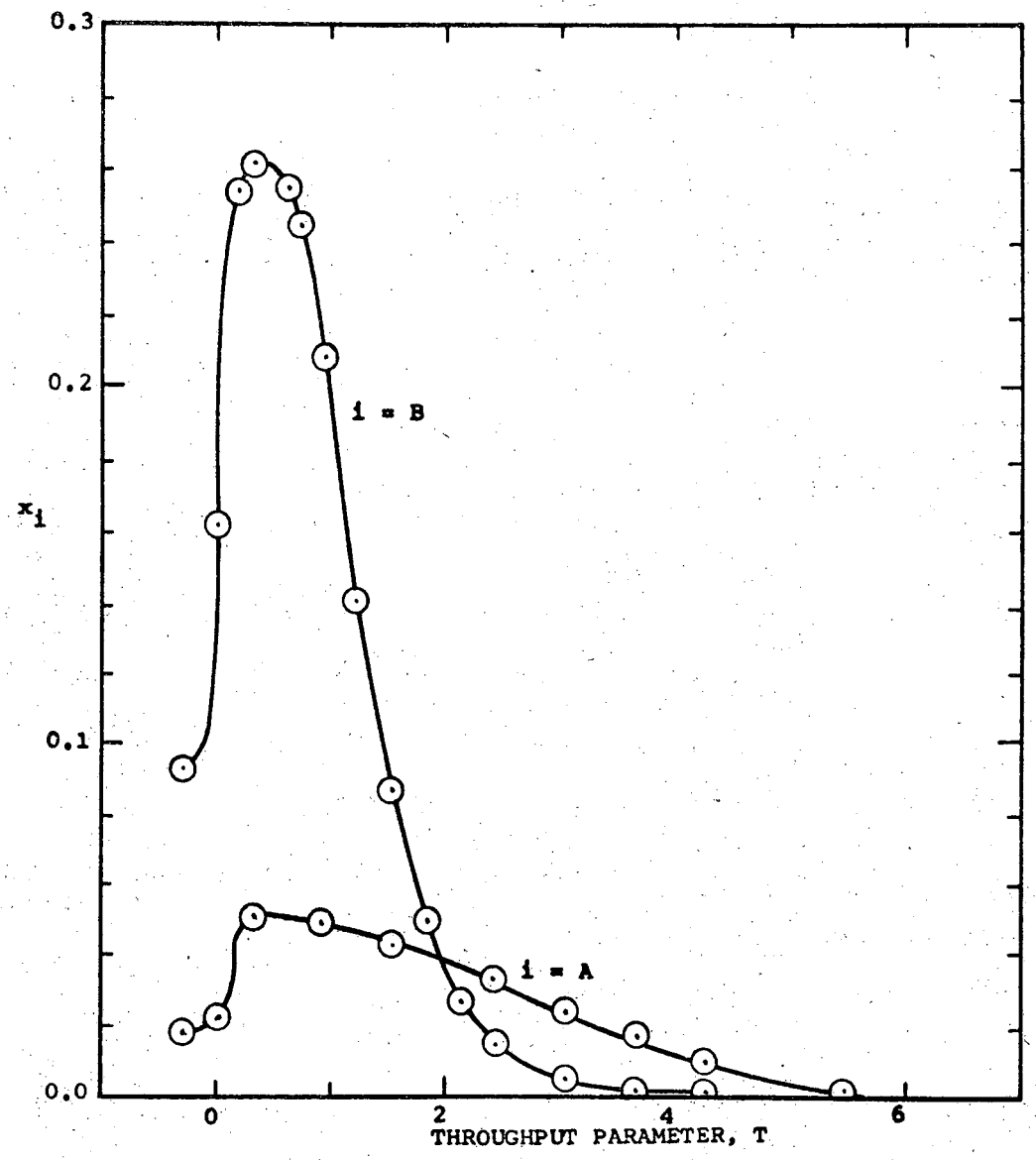

RESIN REGENERATION BY SODIUM IN COLUMN UNIFORMLY PRESATURATED WITH SEA WATER: CALCIUM AND MAGNESIUM EFFLUENT-CONCENTRATION HISTORIES FOR RUN 1RA

FIGURE 15

solid and fluid phase. Figure 16 shows the experimental calcium and magnesium concentration histories together with the theoretical plateaus and transitions (both gradual). Exchange between sodium ions in solution and calcium and magnesium ions in the resin begins after calcium and magnesium effluent concentrations approach the theoretical presaturation plateau concentrations. The predicted magnesium concentration goes to zero during transition 2,3; the predicted calcium concentration, during transition 1,2. Although retarded by mass-transfer inefficiencies, the experimental concentration histories tend to follow the same behavior. The calcium effluent concentration between the regenerant fluid front and the feed plateau appears as a single transition which is, in reality, a compound transition. The overlapping of transition 2,3 and 1,2 is more evident for this case than for the softening runs discussed previously. In the intermediate plateau region, the equilibrium theory predictions are not approached, because low rates of mass transfer control the shape of the concentration histories.

c. Regeneration Runs (n = 4). Figure 17 shows the experimental calcium breakthrough curve for Run 3R (no data were taken for the magnesium breakthrough) together with concentration levels and transitions predicted by equilibrium theory. Complete results for all runs of this type are given in Tables II-c and III-c. At low total

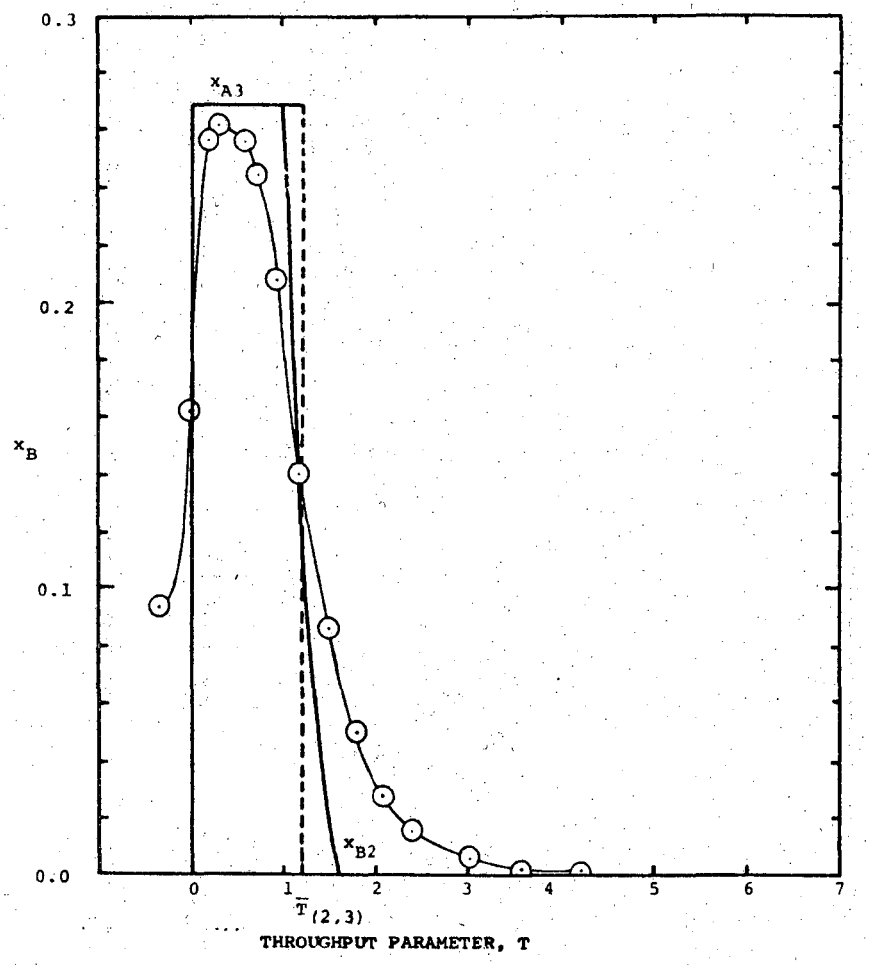

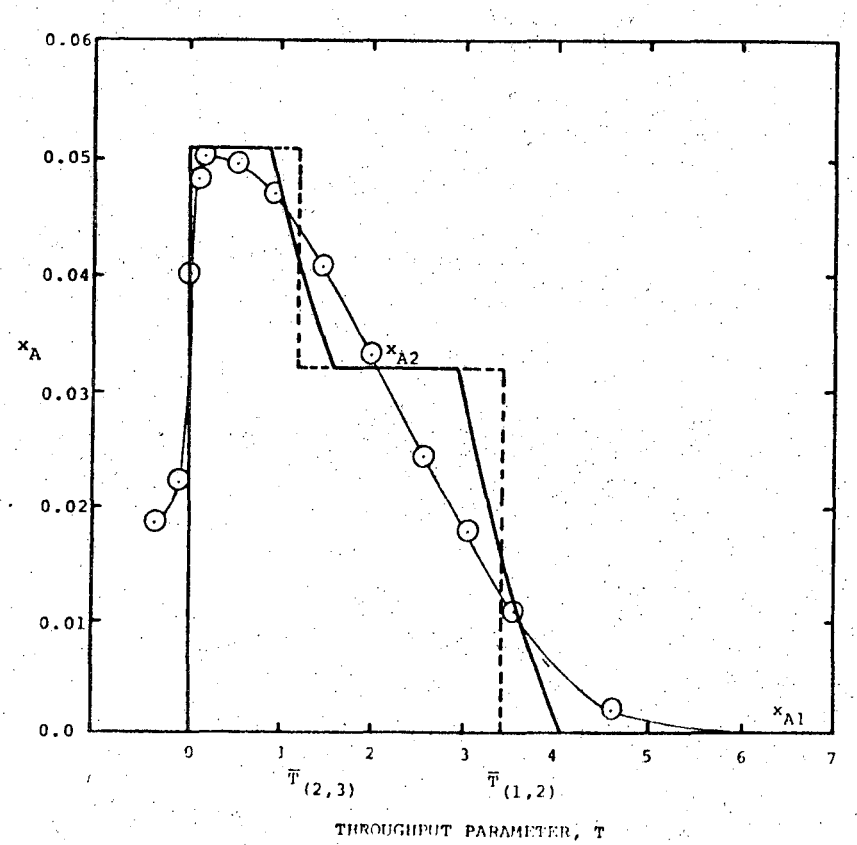

PREDICTED PLATEAUS AND TRANSITIONS (SOLID LINES) COMPARED TO EXPERIMENTAL CALCIUM AND MAGNESIUM EFFLUENT-CONCENTRATION HISTORIES FOR RUN 1RA; REGENERATION BY TWICE-CONCENTRATED BRINE

FIGURE 16

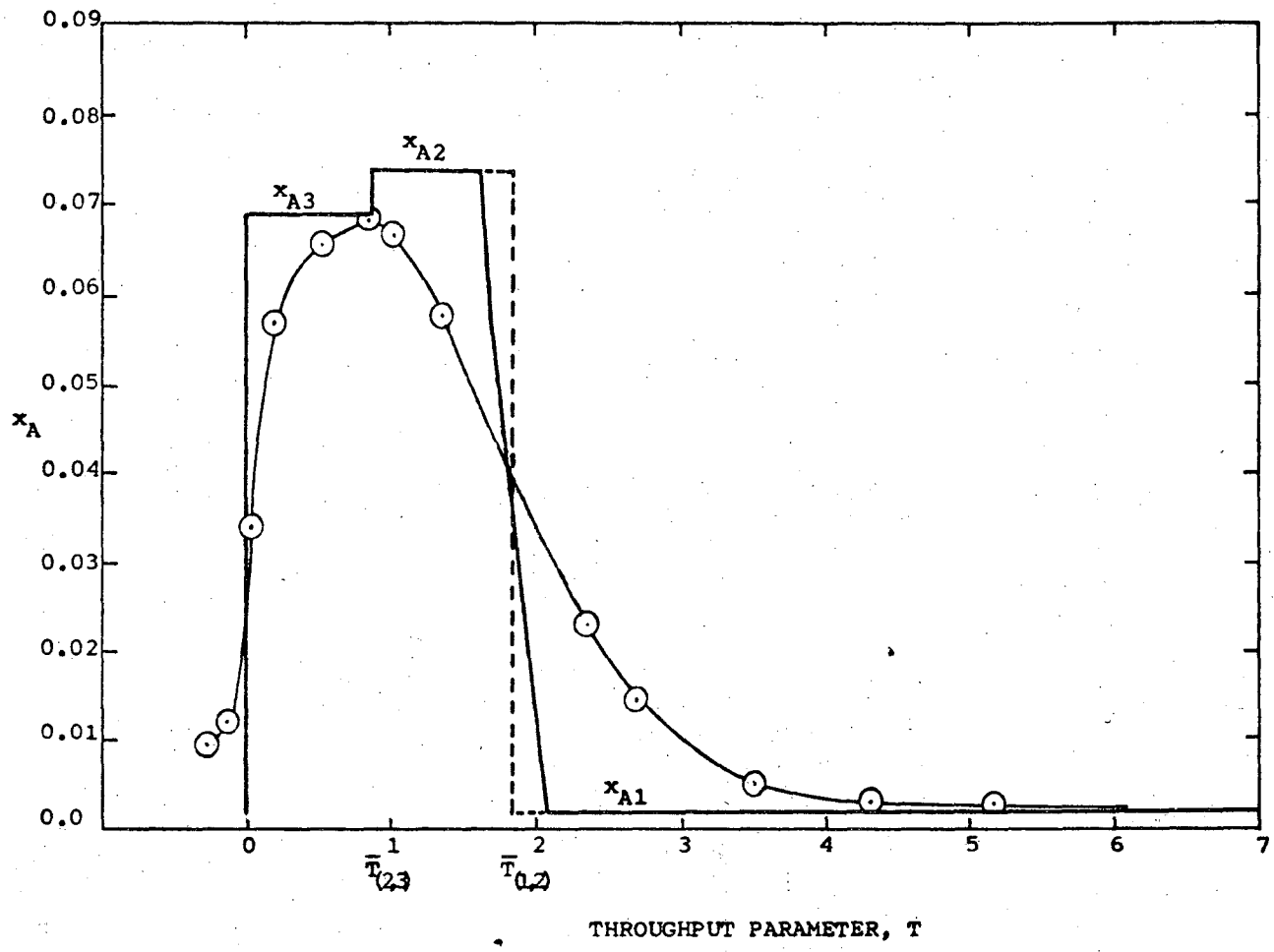

RESIN REGENERATION BY FOUR TIMES CONCENTRATED BRINE IN COLUMN UNIFORMLY PRESATURATED WITH SEA WATER. PREDICTED PLATEAUS AND TRANSITIONS (SOLID LINES) COMPARED TO EXPERIMENTAL CALCIUM EFFLUENT-CONCENTRATION HISTORY FOR RUN 3R

FIGURE 17

solution concentrations, calcium is the ion most favored for uptake by the resin, magnesium next, and sodium least. However, because of the high total solution concentration in this case, the selectivity coefficient of magnesium with respect to sodium becomes less than unity, i.e. sodium is more tightly held by the resin than magnesium. This selectivity reversal leads to equilibrium prediction of an abrupt increase in calcium effluent concentration during transition 2,3 up to the intermediate plateau level and of an abrupt decrease in magnesium concentration, to a level below the feed plateau. The equilibrium behavior predicts a gradual 1,2 transition. As the experimental calcium effluent concentration history approaches the presaturation plateau, the predicted 2,3 transition is ignored, and an apparently single transition starts from the presaturation plateau to reach the calcium feed concentration in the first plateau region.

B. Rate Behavior

The experimental runs analyzed in Section III-A in light of equilibrium theory are now examined with the criteria set forth in Section III-B to determine the true diffusional behavior of ion-exchange columns.

1. Stoichiometric Match. The essential common factor linking the rate- and equilibrium-behavior treatments is the quantity of material emerging in each run from the column from the beginning of fluid flow to equilibration of the resin. This quantity, as given by the shaded area of Figures 18 and 19 is the same as given by the shaded area of Figures 20 and 21. The former represent experimental calcium-breakthrough-curves for saturation and regeneration, respectively, the latter the corresponding calculated equilibrium-theory concentration histories.

Differences in the values of such pairs of experimental and theoretical areas are mainly due to differences between corresponding values of the throughput parameter T calculated from the empirical time- or volume-scale with Equation 27

$$T = \frac{C_o(V - v\epsilon)}{Q\rho_b v} \qquad (27)$$

and the ones derived from equilibrium-theory calculations, dependent only on boundary conditions and exchange capacity values. Therefore, according to the assumption made in Subsection III-A-1, the empirical T scale is not exact and, in order to coincide with the theoretical or "absolute" T scale, has to be modified as follows:

$$T = (T_E - a)b \qquad (71)$$

where T represents the corrected or actual value of T; T_E

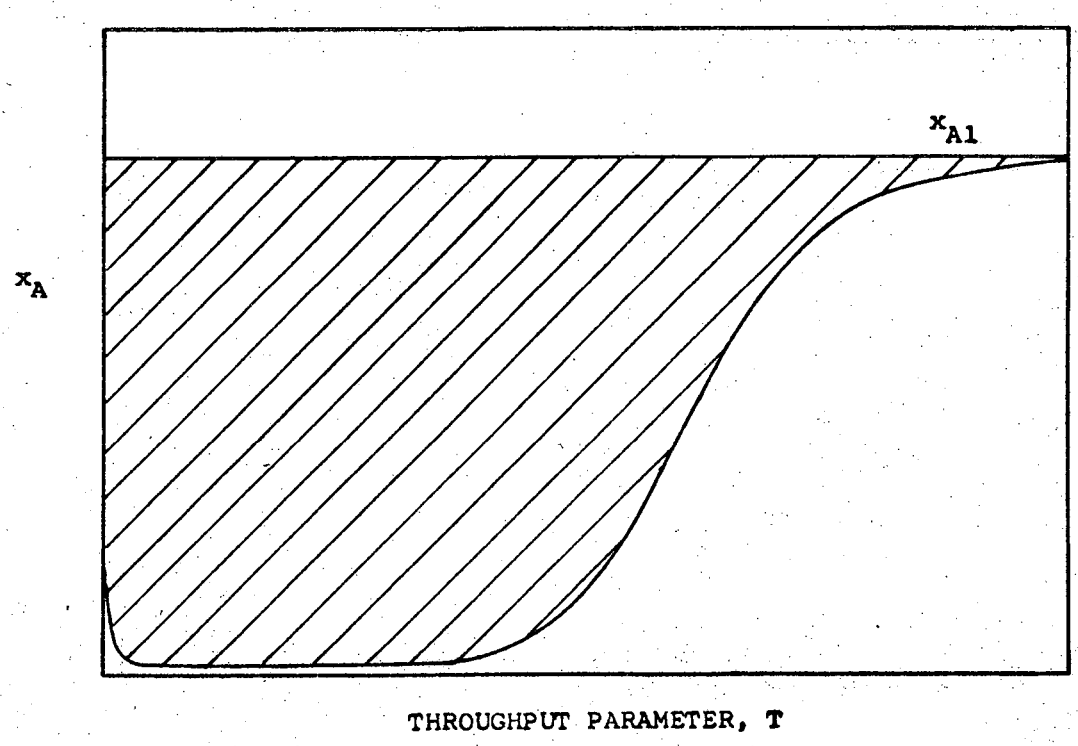

AMOUNT OF CALCIUM (SHADED AREA) IN THE COLUMN, AFTER COMPLETE SATURATION OF COLUMN WITH SEA WATER; SCHEMATIC

FIGURE 18

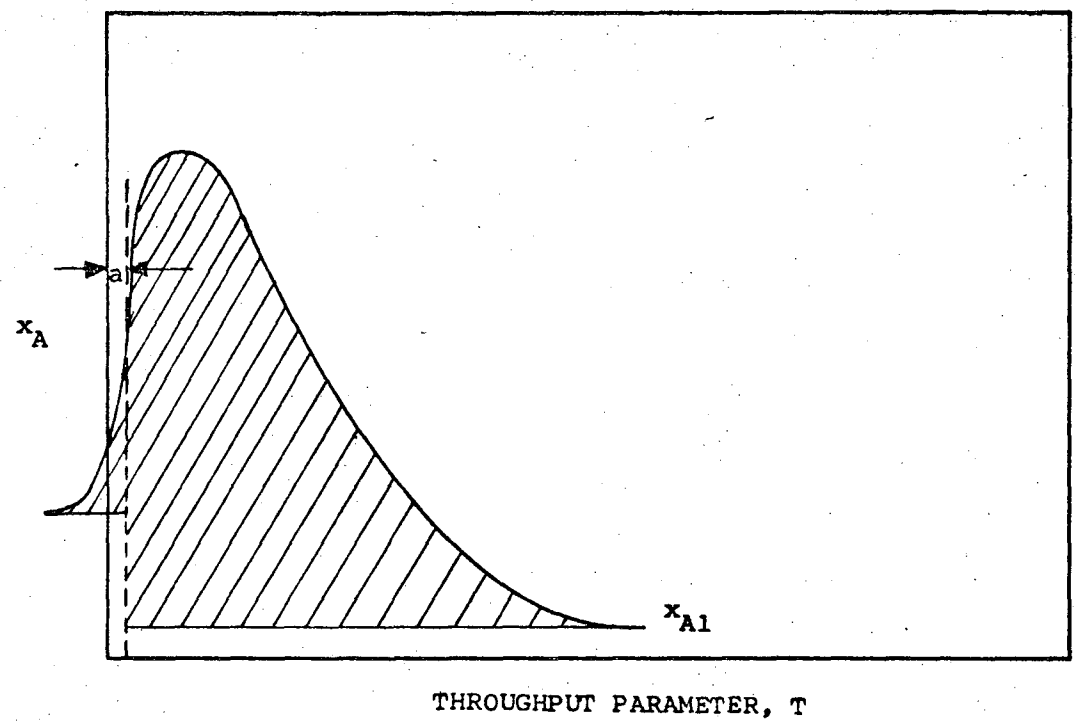

AMOUNT OF CALCIUM (SHADED AREA) IN THE COLUMN, AFTER REGENERATION OF THE COLUMN WITH CONCENTRATED BRINE; SCHEMATIC

FIGURE 19

is the experimentally reported value of T; parameter a identifies the true zero of the T scale with respect to the reported zero; parameter b represents the area ratio A_T/A_E, the theoretical value A_T being given by

$$A_T = \pm \left[(x_{A3} - x_{A2})(\bar{T}_{2,3})_{theor} + (x_{A2} - x_{A1})(\bar{T}_{1,2})_{theor} \right]^{*} \quad (72)$$

and A_E being measured graphically as shown in Figures 18 and 19.

As indicated above, parameter a identifies the position of the stoichiometric center for the initial fluid breakthrough. This initial breakthrough occurs after a softening (or a regeneration) step is interrupted and the flow is reversed in order to start a regeneration (or a softening) step, and it results from displacement of fluid present in the bed void spaces (and in equilibrium with the resin) by the incoming fluid. For the softening step, the stoichiometric center of the fluid-front transition corresponds to the calcium-concentration level midway between x_{AR}, regenerant calcium-equivalent-fraction (or sea-water calcium-equivalent-fraction, x_{Ao}, for the regeneration step) and the minimum (or the maximum) calcium-equivalent-fraction empirically identifiable within the third plateau zone. Table IV shows the values for a and b corresponding to the experimental runs.

2. Kinetic Match. Comparison with theoretical break-

---

*With the present notation, the positive sign holds for regeneration steps, the negative sign for the softening steps.

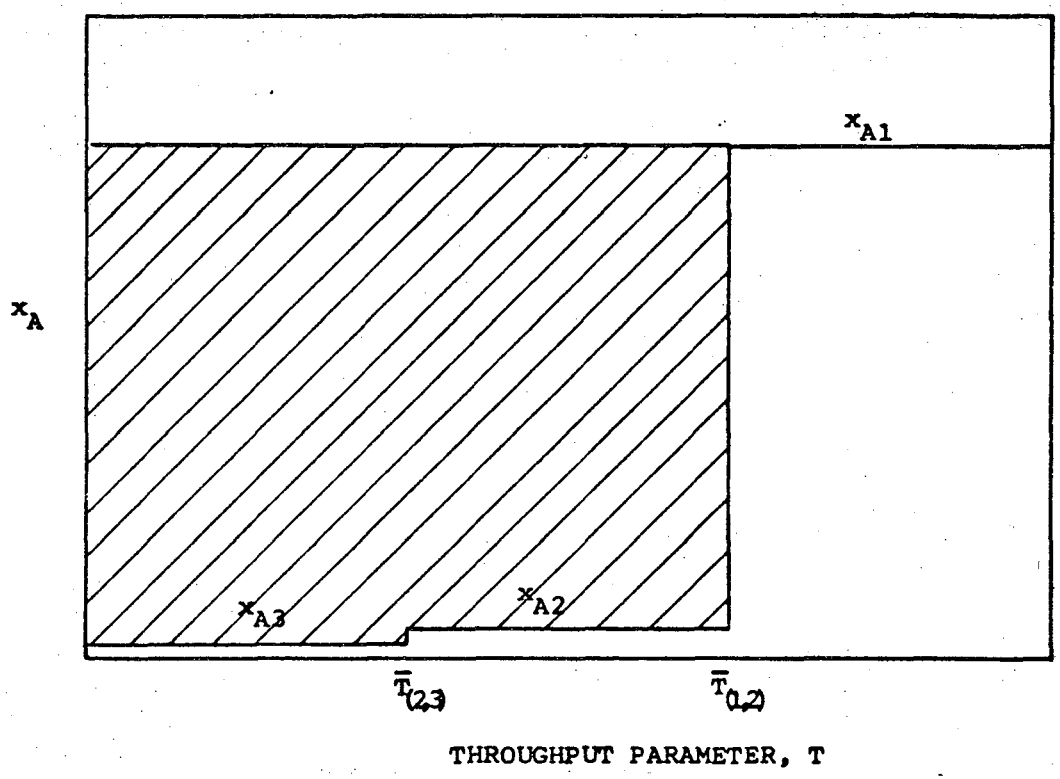

PREDICTED AMOUNT OF CALCIUM (SHADED AREA) IN THE COLUMN, AFTER COMPLETE SATURATION OF COLUMN WITH SEA WATER; SCHEMATIC

FIGURE 20

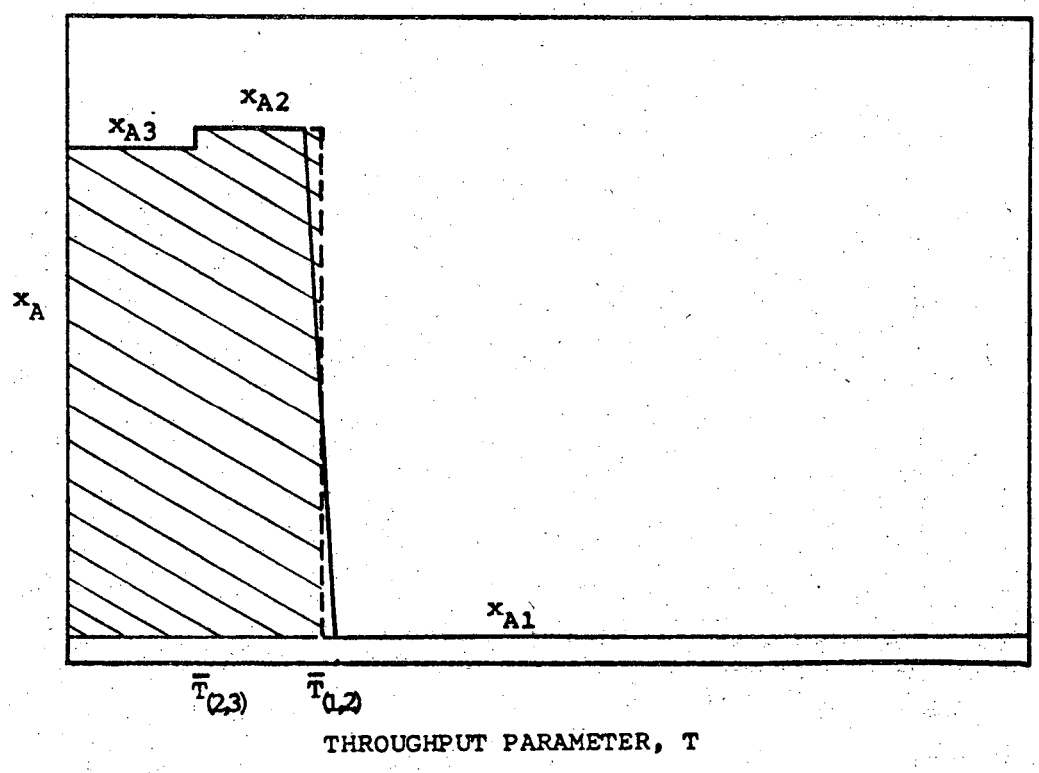

PREDICTED AMOUNT OF CALCIUM (SHADED AREA) IN THE COLUMN, AFTER REGENERATION OF COLUMN WITH CONCENTRATED BRINE; SCHEMATIC

FIGURE 21

TABLE IV

EMPIRICAL PARAMETERS a AND b

a. SATURATION RUNS

RUN	2S	3S	4S	21S
a	0.10	-0.02	0.03	0.00
b	0.9971	0.9748	0.9847	1.024

b. REGENERATION RUNS (n = 2)

RUN	1RA	5R	9R
a	0.10	0.00	0.00
b	0.8536	0.8796	0.8162

c. REGENERATION RUNS (n = 4)

RUN	1R	2R	3R
a	-0.06	0.055	0.07
b	1.027	0.9566	0.9573

through curves given by the reaction-kinetic treatment yields the value of the number of reaction units for each experimental breakthrough curve, provided that the applicable equilibrium parameter is known. Methods to match theory to the simple softening case and to the more complex regeneration cases are indicated below.

a. Saturation Runs. The experimental data of x_A versus T, where A represents calcium, and with the T scale corrected by use of parameters a and b, are first transformed to X versus $\underset{\sim}{T}$. These parameters can be calculated for the 1,2 transition from Equations 14 and 28, respectively:

$$X = \frac{x_A - x_{A2}}{x_{A1} - x_{A2}} \tag{14}$$

$$\underset{\sim}{T} = \frac{T}{\dfrac{y_{A1} - y_{A2}}{x_{A1} - x_{A2}}} = \frac{T}{(\bar{T}_{1,2})_{theor}} \tag{28}$$

Where regeneration has been carried out with concentrated brine containing calcium, the predicted 2,3 transition is not evident from the empirical breakthrough curve; therefore only experimental data falling inside the interval $x_{A2} \leq x_A \leq x_{A1}$, always with $T > (\bar{T}_{2,3})$, are taken into consideration for the kinetic fit of the 1,2 transition. From the transformed data, the slope of the breakthrough curve can be calculated at X = 0.5 and used to determine N_R from Figure 10, at the predicted $R_{1,2}$. With N_R and R, use

of the cross-plots (Figure 9) gives five theoretical values of X versus $\underset{\sim}{T}$. The results are reported in Table V-a. Figures 22 and 23 show the excellent match of the theory to the experiments in the case of Run 4S and 21S; X is on a probability ordinate versus $\underset{\sim}{T}$ on a linear abscissa.

b. Regeneration Runs (n = 2). Transition parameters for the regeneration runs are given by Equation 14,

$$X^{\dagger} = 1 - X = \frac{x_{A1} - x_A}{x_{A1} - x_{A2}} \qquad (14)$$

with $X^{\dagger}$ ranging from unity to zero, and by equation 28. In these runs, the intermediate or second plateau as predicted by the theory is completely obliterated in the empirical effluent-concentration history. The 2,3 and 1,2 transitions are very close together and the low mass-transfer rates involved cause them to overlap, so that the effluent-concentration history appears as a single change, as shown in Figure 15.

High mass-transfer rates would cause only a light spreading around the stoichiometric center of each transition, as depicted schematically in Figure 24, thus allowing the intermediate plateau to develop clearly. Low mass-transfer rates bring about a much more extended spreading, and the experimental results do not conform at all to the equilibrium requirement of the existence of the intermediate plateau. The inferred "overlap" signifies that the theoretical rate-

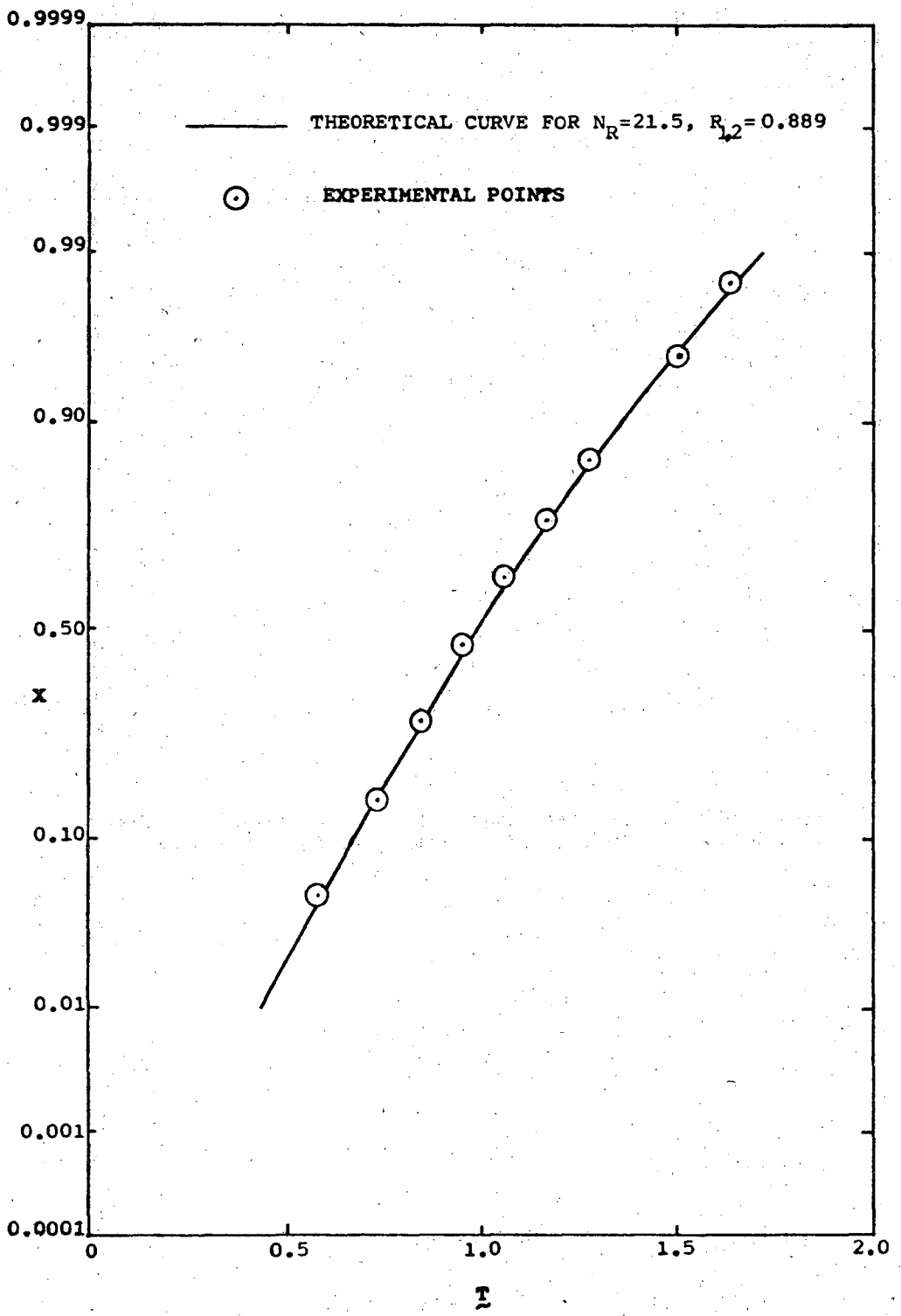

MATCH OF NORMALIZED CALCIUM 1,2-TRANSITION TO GENERALIZED REACTION-KINETIC BINARY MASTER CURVES FOR RUN 4S

FIGURE 22

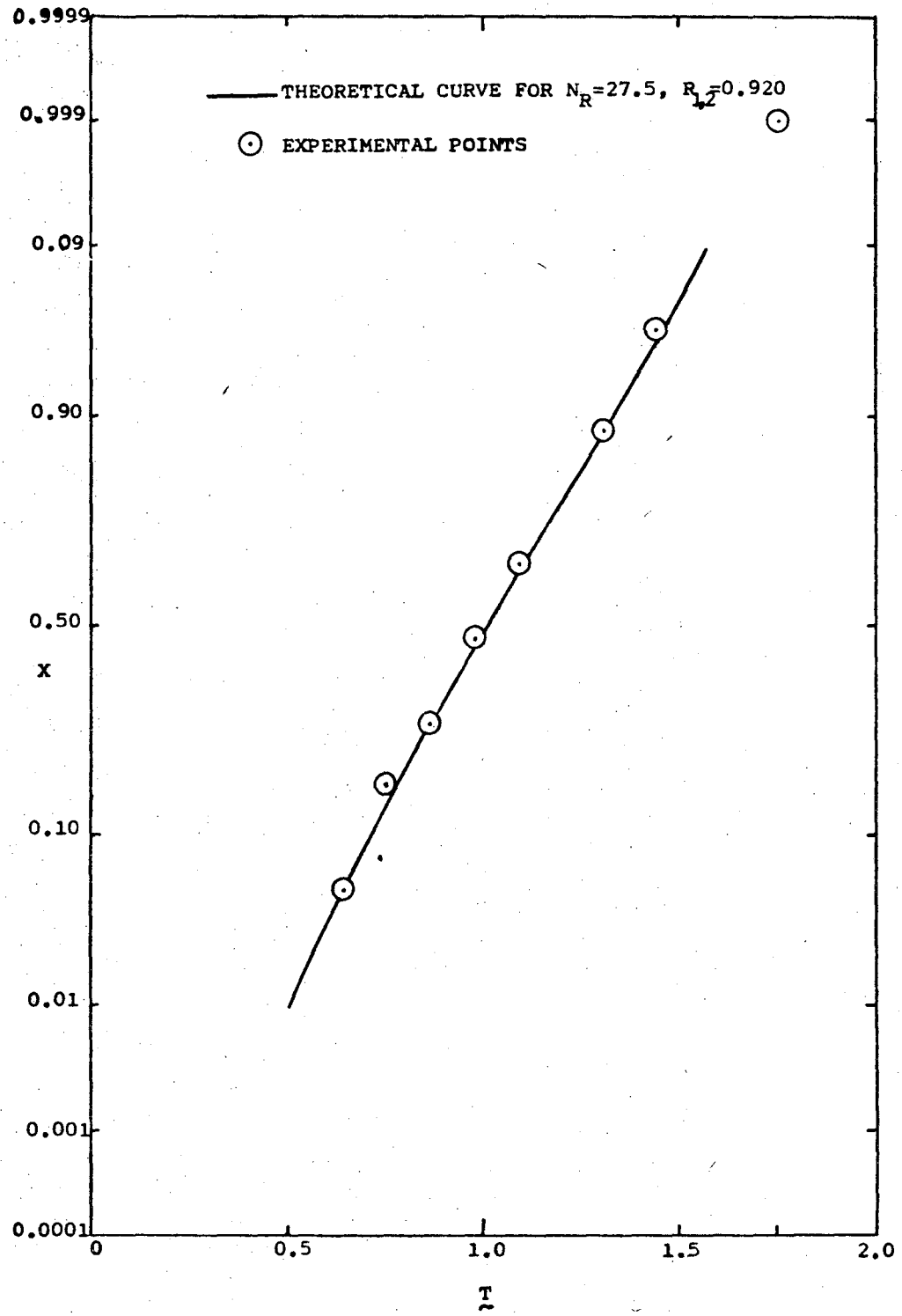

MATCH OF NORMALIZED CALCIUM 1,2-TRANSITION TO GENERALIZED REACTION-KINETIC BINARY MASTER CURVES FOR RUN 21S

FIGURE 23

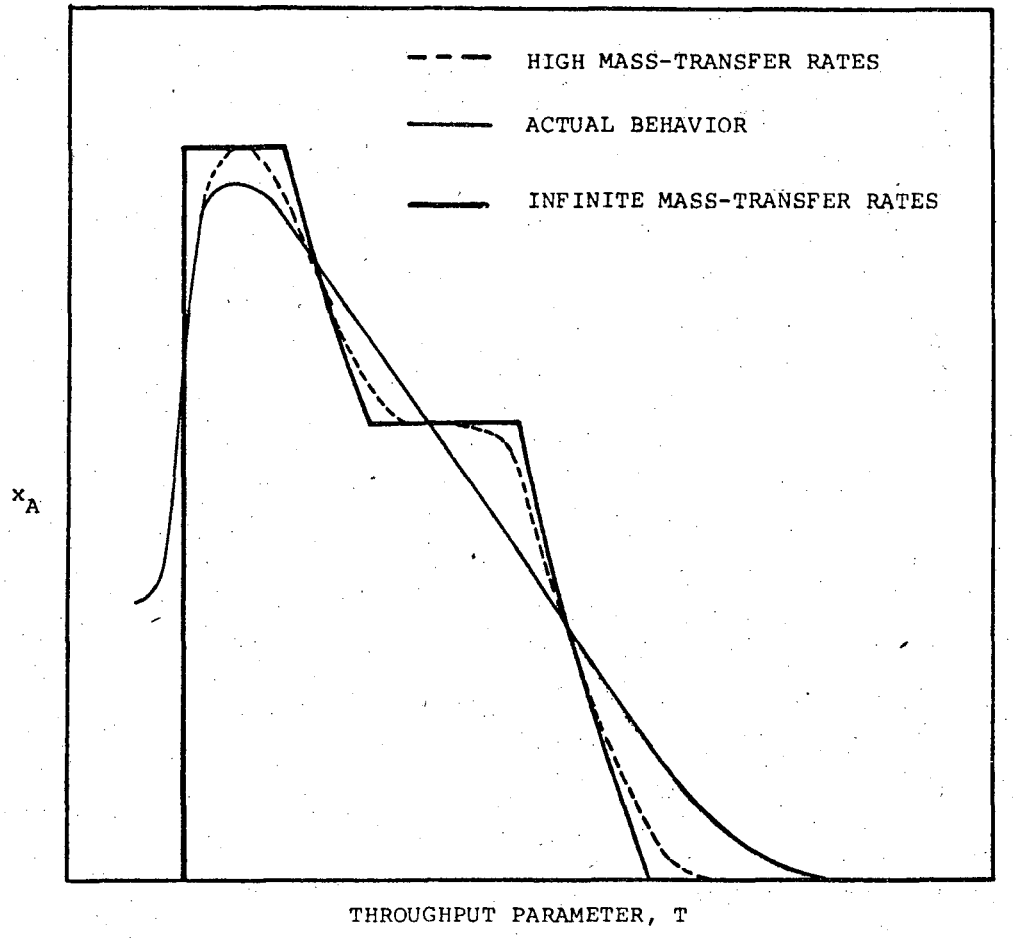

EFFECT OF MASS-TRANSFER RATES ON CALCIUM BREAKTHROUGH CURVES FOR EACH TRANSITION (REGENERATION WITH TWICE-CONCENTRATED BRINE)

FIGURE 24

TABLE V

NUMBERS OF REACTION UNITS FROM GENERALIZED REACTION-KINETIC CURVES MATCHED TO EXPERIMENTAL CALCIUM BREAKTHROUGH CURVES

a. SATURATION RUNS

RUN	2S	3S	4S	21S
$\Delta x_{0.5}/\Delta \underset{\sim}{T}$	1.15	1.35	1.44	1.59
$R_{1,2}$	0.887	0.890	0.889	0.920
N_R	12.0	18.0	21.5	27.5

b. REGENERATION RUNS (n = 2)

RUN	1RA	5R	9R
$R_{1,2}$	1.175	1.190	1.23
N_R	24.0	16.0	9.1

c. REGENERATION RUNS (n = 4)

RUN	1R	2R	3R
$R_{1,2}$	1.13	1.123	1.124
N_R	2.5	4.2	14.0

controlled breakthrough curve for the 1,2 transition begins long before the corresponding 2,3 curve is complete, so that two different values of x_A (one above and one below x_{A2}) would be predicted at the same T. Therefore, any match of breakthrough to master curves for the purpose of determining the number of reaction units must be limited to $T \geq (\bar{T}_{1,2})_{theor}$ for the 1,2 transition (or possibly also to $T \leq (\bar{T}_{2,3})_{theor}$ for the 2,3 transition, although a match here did not prove feasible).

The results are given in Table V-b. Figure 25 shows the match between the experimental data inside the interval $x_{A2} \leq x_{A1} \leq x_{A1}$ and theoretical breakthrough curves for Run 1RA on the usual $X^{\dagger}$ probability plot versus linear $\underset{\sim}{T}$ scale. Departures from theoretical behavior appear at values of $X^{\dagger}$ approaching zero, which may be attributed to experimental errors in measuring small concentrations or to nonuniformity in resin properties. It is to be noted that a good match is also obtained for the range of data points with $T \leq (\bar{T}_{1,2})_{theor}$.

c. <u>Regeneration Runs (n = 4)</u>. For high mass-transfer rates (along with axial dispersion, which controls the initial fluid-front breakthrough), three breakthrough curves are predicted for the three transitions, as shown in Figure 26. The single true-concentration history (solid curve) corresponds to the combined effect of these predictions. The selectivity reversal for magnesium, discussed previously, requires an increase in the theoretical calcium effluent concentration

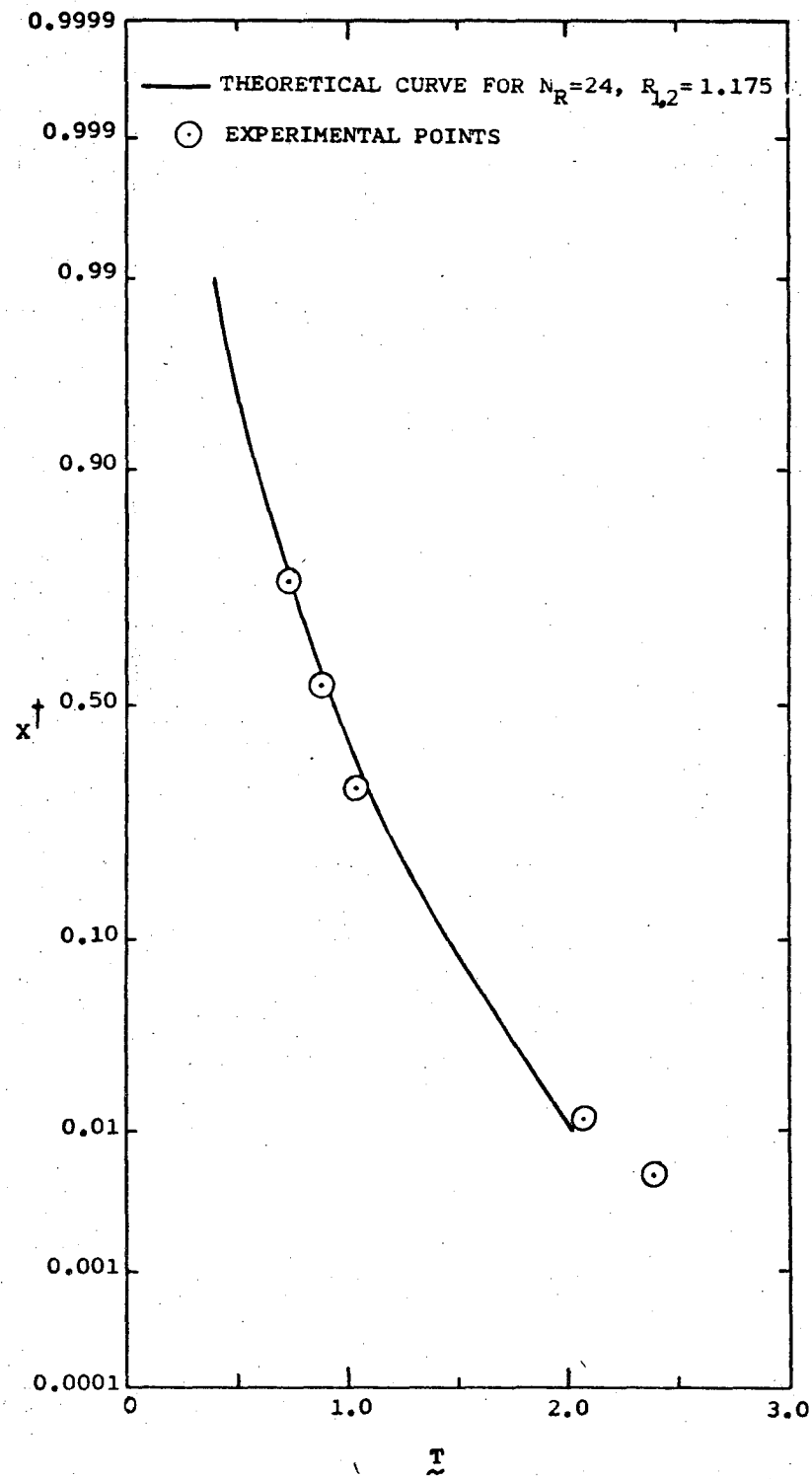

MATCH OF NORMALIZED CALCIUM 1,2-TRANSITION TO GENERALIZED REACTION-KINETIC BINARY MASTER CURVES RUN 1RA

FIGURE 25

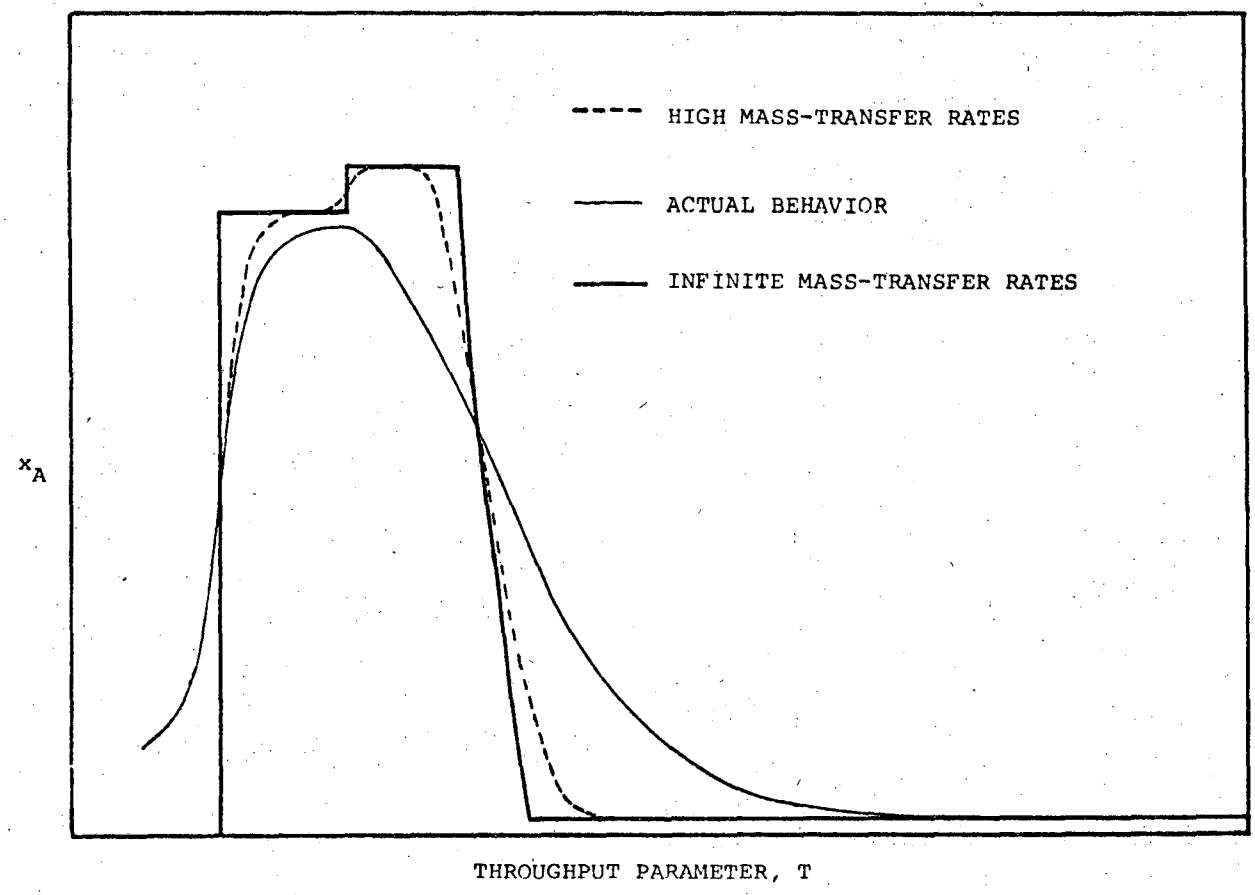

EFFECT OF MASS-TRANSFER RATES ON CALCIUM BREAKTHROUGH CURVES FOR EACH TRANSITION
(REGENERATION WITH FOUR TIMES CONCENTRATED BRINE)

FIGURE 26

during the 2,3 transition. This predicted 2,3 transition should start at a T value near $(\bar{T}_{2,3})_{theor}$, and the concentration should rise from the third-plateau to the second-plateau level. However, this transition is overshadowed by the following 1,2 transition, centered at $(\bar{T}_{1,2})_{theor}$, and the measured experimental concentrations do not approach the second-plateau level at all.

As in the previous cases, the kinetic match is attempted only in the range of concentration with $T \geq (\bar{T}_{1,2})_{theor}$. Figure 27 shows the results for Run 3R, where it appears that a good match results also in the region where $T < (\bar{T}_{1,2})_{theor}$. The complete results for this case are reported in Table V-c.

3. Controlling Resistances. The following numerical values for the various parameters involved are believed representative for Duolite C-25 ion-exchange resin and the sea-water solutions under consideration:

a. $\bar{c}$ = 3.0 (ion equivalents/liters of solid) concentration of active sites on the solid (8).

b. D_p/D_f, ratio of solid- to liquid-phase diffusivity, in the range of 10^{-1} (8,19).

c. D_f, fluid-phase diffusivity, estimated at 1.5×10^{-5} cm^2/sec (8).

d. d_p, average particle diameter, 0.061 cm.

The volume of a particle v_p is given by the sum of solid volume and of pore volume, with $v_{solid} = (1 - \chi)v_p$ and $v_{pore} = \chi v_p$, where χ is the internal porosity of the particle.

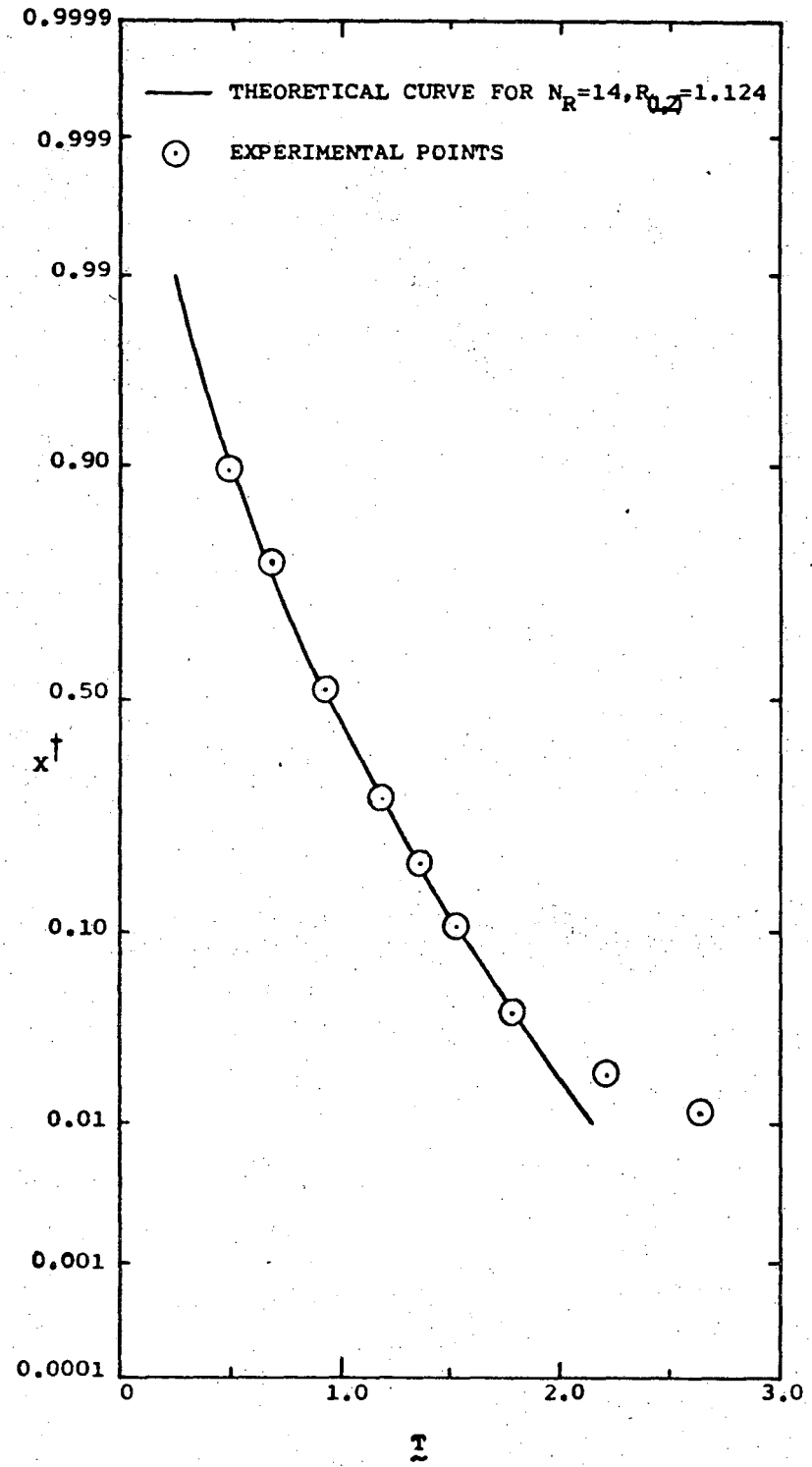

MATCH OF NORMALIZED CALCIUM 1,2-TRANSITION TO GENERALIZED REACTION-KINETIC BINARY MASTER CURVES FOR RUN 3R

FIGURE 27

The diffusion-effective concentration of the particle is given by:

$$\bar{c}_{eff} = (1 - \chi)\bar{c}_{app} + \chi\bar{c}_{pore} \tag{73}$$

where $\bar{c}_{app}$ is the apparent ion-equivalent concentration of the solid portion of a particle given by

$$\bar{c}_{app} = \bar{c}(D_p/D_f) \tag{74}$$

Stated differently, in order to model the diffusional rate behavior inside the particle, the solid with site concentration $\bar{c}$ and diffusivity D_p is considered a liquid of diffusivity D_f, for which the average concentration $\bar{c}_{app}$ will give the same flux of material.

As mentioned earlier, Duolite C-25 specifications indicate a closed-pore structure. The total concentration of the fluid phase inside the pores is considered to lag behind the concentration of bulk fluid flowing outside the particle. To simplify the problem, it may be assumed that for each cycle of saturation and regeneration, the fluid concentration inside the pores remains constant at an average level weighted by the relative saturation and regeneration times. The present experiments, however, appear to show no effect whatever of pore concentration on diffusion rate; therefore the term $\bar{c}_{pore}$ can be dropped from the right-hand side of Equation 73, and since $\chi << 1$,

$$\bar{c}_{eff} = \bar{c}_{app} = \bar{c}(D_p/D_f) \tag{74a}$$

For solid-transport controlling, the diffusional contour lines inside the envelope of Figure 8 are defined by the parameter $(\psi_p \underset{\sim}{\Lambda} D_p)/D_f$. In the present study, $\psi_p \cong 1$, since the equilibrium parameter is close to unity in both the saturation and the regeneration cases. The definition of $\underset{\sim}{\Lambda}$ (Equation 26) can be related to $\bar{c}$ and to $\bar{c}_{app}$,

$$\underset{\sim}{\Lambda} = \bar{T}\Lambda = \bar{T}\frac{Q\rho_b}{C_o n} = \bar{T}\frac{(1-\epsilon)\bar{c}}{C_o n} \tag{75}$$

where $\bar{T} = (y'' - y')/(x'' - x')$ is the stoichiometric center of the transition under consideration, n (= 1,2,4) the concentration factor, ϵ (= 0.40) is the interparticle void fraction, C_o (= 0.62N) normal sea-water concentration, and Q, ρ_b, and $\bar{c}$ have already been defined. Substituting Equation 74 into Equation 75 gives,

$$\underset{\sim}{\Lambda} = \bar{T}\,\frac{1-\epsilon}{C_o n}\,\bar{c}_{app}\,(D_f/D_p) \tag{76}$$

or,

$$\frac{\underset{\sim}{\Lambda} D_p}{D_f} = \bar{T}\,\frac{1-\epsilon}{C_o n}\,\bar{c}_{app} \tag{77}$$

Table VI gives the values of $N_R d_p/h$ and $(d_p F/S)D_f$ calculated from the empirical and estimated data for the various cases of saturation and regeneration. These results are plotted

TABLE VI

ESTIMATED HEIGHTS OF REACTION UNITS AND PÉCLET NUMBERS FOR FLOW

a. SATURATION RUNS

RUN	2S	3S	4S	21S
F/S, gal/(ft^2 min)	8.0	5.0	4.0	3.0
N_R	12.0	18.0	21.5	27.5
$N_R d_p/h$	0.0060	0.009	0.0110	0.0148
$d_p(F/S)/D_f$	2200.0	1380.0	1100.0	830.0

b. REGENERATION RUNS (n = 2)

RUN	1RA	5R	9R
F/S, gal/(ft^2 min)	1.0	2.84	4.1
N_R	24.0	16.0	9.1
$N_R d_p/h$	0.012	0.008	0.0046
$d_p(F/S)/D_f$	276.0	780.0	1130.0

c. REGENERATION RUNS (n = 4)

RUN	1R	2R	3R
F/S, gal/(ft^2 min)	4.0	2.0	0.5
N_R	2.5	4.2	14.0
$N_R d_p/h$	0.00125	0.0021	0.007
$d_p(F/S)/D_f$	1100.0	550.0	138.0

over a limited range of the general-correlation graph in Figure 28; an empirical value for $(\underset{\sim}{\Lambda} D_p/D_f)_{sat}$ can be evaluated from the plotted saturation points. The theoretical values for the diffusional parameter in the regeneration cases, corresponding to the above $(\underset{\sim}{\Lambda} D_p/D_f)_{sat}$ are given by

$$\left(\underset{\sim}{\Lambda}\frac{D_p}{D_f}\right)_{reg,n} = \frac{1}{n}\left(\frac{\bar{T}_{reg}}{\bar{T}_{sat}}\right)\left(\underset{\sim}{\Lambda}\frac{D_p}{D_f}\right)_{sat} \tag{78}$$

On fitting the experimental points for saturation empirically to a constant diffusional contour line, a value of $(\underset{\sim}{\Lambda} D_p/D_f)_{sat} = 0.230$ is determined. The corresponding ratio $D_p/D_f = 0.02$ of particle- to fluid-phase diffusivity agrees favorably with the predicted range of values for this ratio. Use of Equation 78 gives the following values for $\underset{\sim}{\Lambda} D_p/D_f$:

$$n = 2 \qquad (\underset{\sim}{\Lambda} D_p/D_f)_{reg,2} = 0.094$$

$$n = 4 \qquad (\underset{\sim}{\Lambda} D_p/D_f)_{reg,4} = 0.0265$$

The constant lines corresponding to the empirical saturation value and to the predicted regeneration values are shown in Figure 28.

The saturation points for both n = 2 and n = 4 agree within 1%. For regeneration runs with n = 2, the average

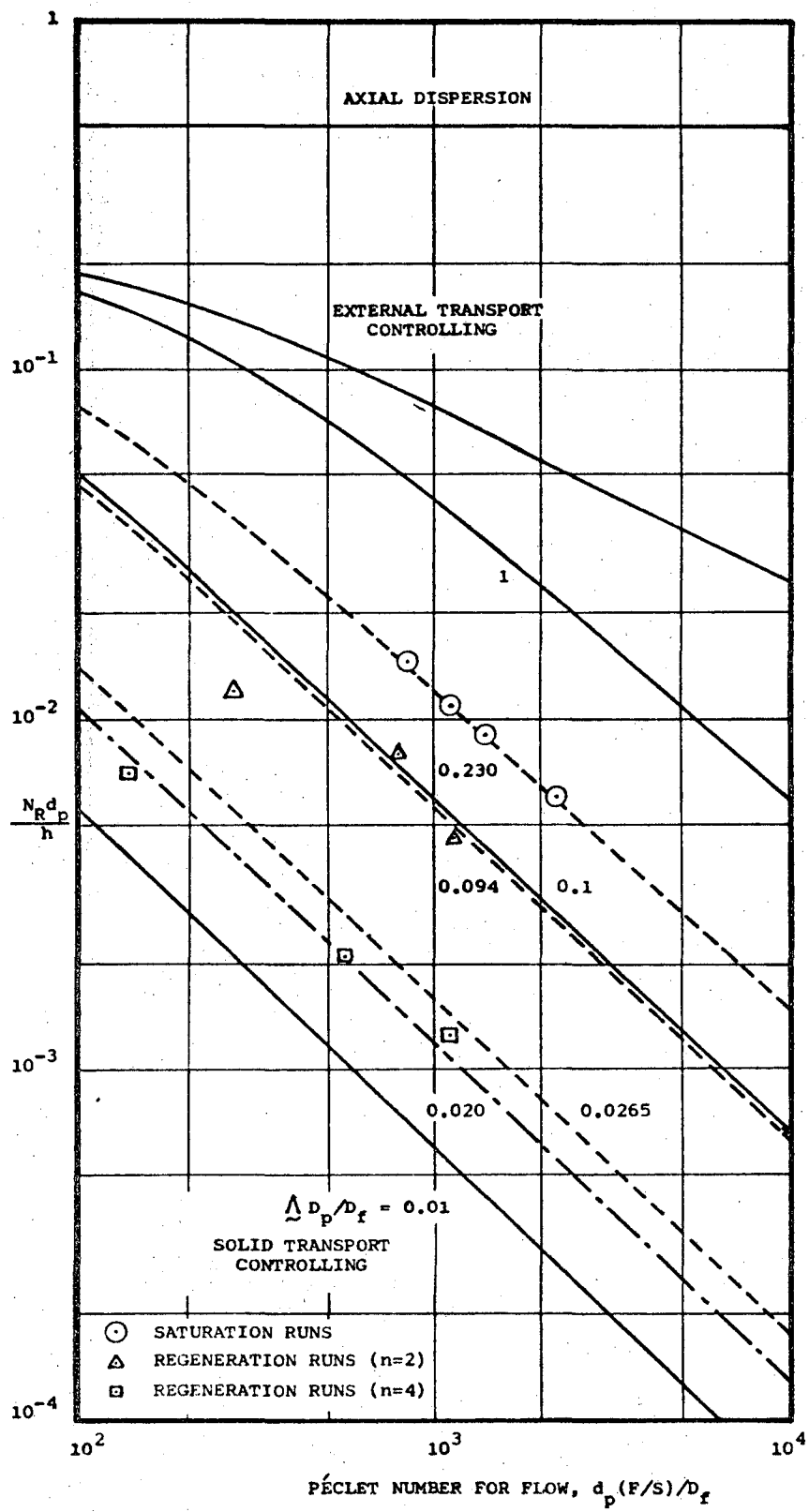

COMPARISON OF EXPERIMENTAL RESULTS WITH GENERAL CORRELATION

FIGURE 28

deviation is about 20%. Therefore, the predicted $\underset{\sim}{\Lambda} D_p/D_f = 0.094$ appears to represent these runs adequately. In the case of regeneration runs with $n = 4$, the plotted points fit a diffusional contour line characterized by $\underset{\sim}{\Lambda} D_p/D_f = 0.020$, which is about 23% below the prediction. The internal consistency of the three points for $n = 4$ suggests that the method developed above for interpreting compound transitions yields estimates of the regeneration performance more conservative than would be predicted from the corresponding saturation step at the same flow rate.

The only known way of solving compound transitions is that of computer calculations using the method of characteristics. To resolve fully the above uncertainties, such computations should be made to determine concentration histories for both the predicted and the observed transport ratios, so that results for both can be compared with the experimental curve.

4. Internal and External Resistances. It has been shown in the previous paragraph that fluid-phase pore diffusion is negligible compared with solid-phase diffusion for saturation runs and for regeneration runs; some further investigation is needed to resolve the uncertainties for regeneration runs.

It is of interest to break down the apparent resistance, now labeled as internal resistance, into internal and external resistances, in order to determine the relative

importance of the latter in the case of the saturation runs.

When external mass-transfer only is controlling, the relationship between the number of transfer units and the flow rate is given by

$$N_f = (F/S)^{-1/2} \tag{79}$$

When internal (particle, in this instance) diffusion only controls,

$$N_p = (F/S)^{-1} \tag{80}$$

Therefore, for any combination of external transport and internal diffusion controlling the rate of ion exchange, the relationship should be given by:

$$N_{of} = (F/S)^{-B} \tag{81}$$

or

$$N_{op} = (F/S)^{-B} \tag{82}$$

where the exponent B ranges between 1/2 and 1, and is indicative of the relative percentage of external and internal resistances. Figure 29 shows a logarithmic plot of N_R (related to N_{of} and N_{op} by Equation 67) versus F/S. The slope of the solid line fitting the points is B =-0.875, corresponding to a 3 to 1 ratio of internal to external transport.

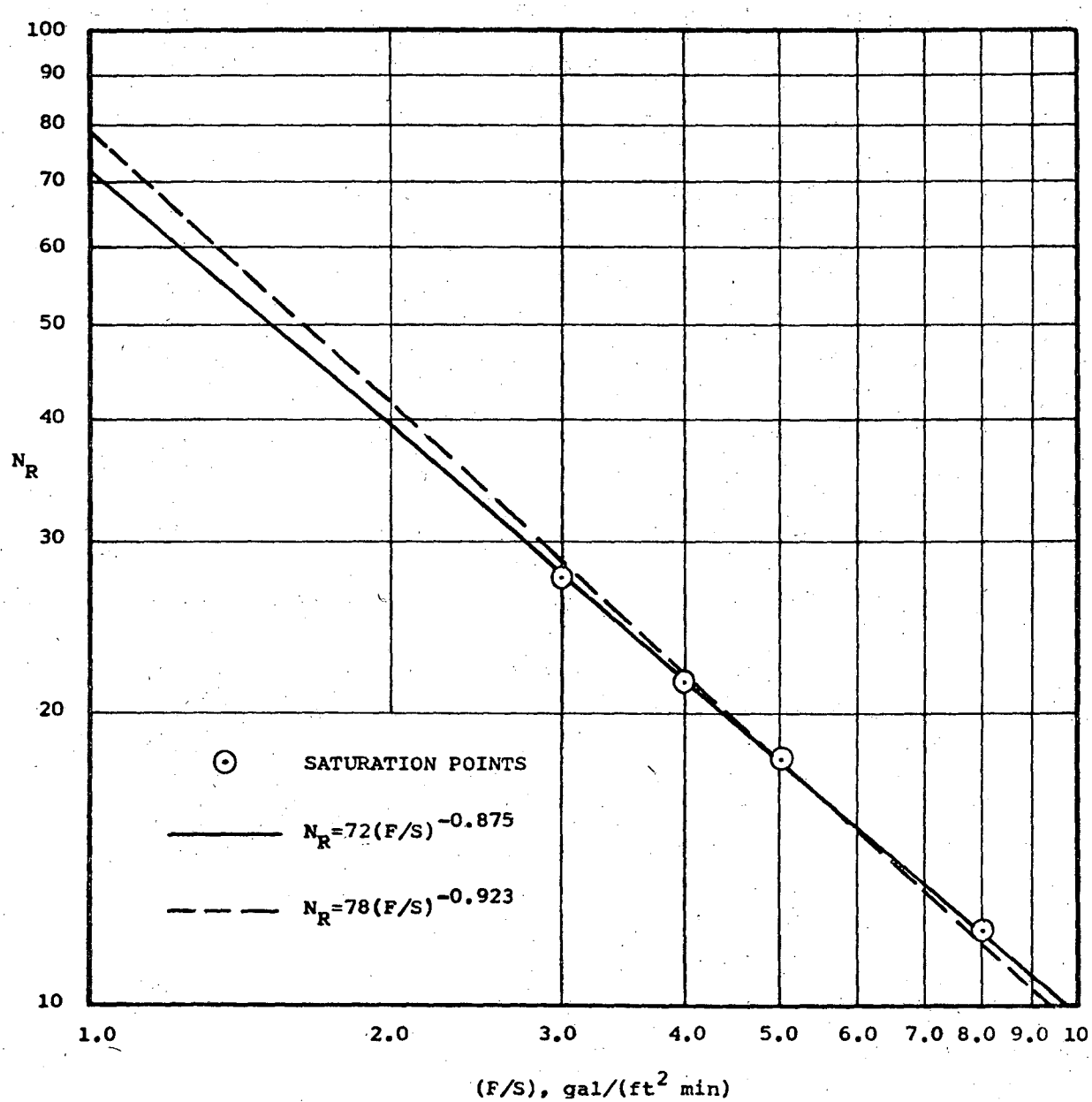

CORRELATION OF NUMBER OF REACTION UNITS AND FLOW RATE FOR SATURATION RUNS

FIGURE 29

The relative percentage of internal and external resistances constituting the overall resistance can be determined by a theoretical procedure. Axial dispersion, external mass transfer, and internal diffusion act in series; the overall resistance can be expressed as

$$\frac{1}{N_R} = \left(\frac{1}{N_d} + \frac{1}{N_f} + \frac{1}{N_p}\right)\left(\frac{R + 1}{2}\right) \tag{83}$$

or

$$\frac{h}{N_R d_p} = \left(\frac{h}{N_d d_p} + \frac{h}{N_f d_p} + \frac{h}{N_p d_p}\right)\left(\frac{R + 1}{2}\right) \tag{84}$$

where the only unknown is $(h/N_p d_p)$, since $(h/N_R d_p)$ and $(R + 1)/2$ have been calculated, and axial dispersion and external resistances are evaluated from the diagram of Figure 28. Table VII gives the values of the individual resistances as percentages of the resistance given by internal diffusion, for each saturation run. The average percentage of internal resistance corresponds to a $B = -0.923$. The dashed line given by $N_{op} = (F/S)^{-0.923}$ drawn on Figure 29 also agrees with the experimental points to within the accuracy of Equation 84 and of the flow measurements.

TABLE VII

INDIVIDUAL STEP CONTRIBUTIONS TO APPARENT OVERALL MASS-TRANSFER RESISTANCE

RUN	2S	3S	4S	21S
$d_p(F/S)/D_f$	2200.0	1380.0	1100.0	830.0
$h/N_R d_p$	166.0	111.0	89.3	69.0
$h/N_d d_p$	2.0	2.0	2.0	2.0
$h/N_f d_p$	18.85	15.15	13.52	11.77
$h/N_p d_p$	154.0	100.0	78.28	52.60
% of resistance given by internal diffusion	88.2	85.4	84.4	81.0

Average % of resistance given by internal diffusion: 84.7

IV. SUMMARY AND CONCLUSIONS

1. Effluent-concentration histories for calcium and magnesium in sea-water softening and exhausted-resin regeneration runs have been compared to the corresponding effluent profiles calculated by equilibrium-theory relations from known calcium-sodium and magnesium-sodium selectivity coefficients. To unify the treatment of the experimental data, average values of selectivity coefficients were adopted for use in all the equilibrium calculations. Small deviations were arbitrarily attributed to differences in the weight of resin filling the laboratory column during each set of runs, and to changes in the total solution normality.

2. Calculated presaturation and intermediate plateau compositions appear to represent limiting values for the constant composition zones identifiable in the experimental effluent-concentration histories. These limits are approached in the presaturation plateau zone in all cases; only for saturation runs does the intermediate-plateau concentration-level represent a limiting value. For all regeneration runs, the shapes of the experimental concentration histories are determined by rate-limiting behavior to a larger extent than for the saturation runs; the calcium transition between presaturation and intermediate plateaus is overshadowed by

the preceding inert fluid-front breakthrough and by the following transition between intermediate and feed plateaus.

3. Analysis of the experimental runs has been made with the reaction-kinetic model to determine the true diffusional behavior controlling the shape of the concentration histories. Matching normalized calcium transitions between the intermediate and the feed plateaus to generalized solutions of the reaction kinetic model gave the average numbers of reaction units (or of the mass-transfer coefficients).

4. On the basis of Duolite C-25 specifications indicating a closed pore-structure, fluid-phase pore diffusion has been assumed to be negligible as compared to solid-phase diffusion. The assumption has been verified within 1% for the saturation runs; 20% for regeneration runs with $n = 2$; 23% for regeneration runs with $n = 4$. The last uncertainties can be resolved by computer calculations reproducing the experimental effluent-concentration histories from either the estimated or the empirical mass-transfer coefficient.

5. Examination of the numbers of reaction units in terms of a general correlation indicates that 85% of the apparent resistance due to internal (particle) mass-transfer resistance, with the remaining 15% attributable to external resistance and axial dispersion.

ACKNOWLEDGMENT

This report was prepared under the auspices of the U. S. Atomic Energy Commission.

Thanks are due to the Office of Saline Water, U. S. Department of the Interior, for financial support of the initial phase of this study. The author is indebted to Professor Theodore Vermeulen and Gerhard Klein for guidance and advice, and to Professor Alan D. K. Laird, Director of the Sea Water Conversion Laboratory. The assistance of Mrs. Mary Ellen Sassi with the manuscript is affectionately acknowledged.

T	Throughput parameter defined by Equation 27
$\bar{T}$	Stoichiometric value of throughput parameter for transitions between contiguous plateau zones
$\underset{\sim}{T}$	Throughput parameter for a transition
V	Feed-solution volume
v	Column volume
v_p	Particle volume
X	Transition parameter for fluid phase
x_i	Equivalent fraction of species i in fluid phase
Y	Transition parameter for exchanger phase
y_i	Equivalent fraction of species i in exchanger phase
α_{ij}	Separation factor
ϵ	Column void fraction
Λ	Partition ratio
$\underset{\sim}{\Lambda}$	Partition ratio for a transition
ν_i	Absolute value of valence of species i
ρ_b	Resin bulk density
ψ_p	Correction factor in Equation 61
ψ_{pore}	Correction factor in Equation 56
χ	Intraparticle porosity

REFERENCES

1. Helferrich, F., Ion Exchange, McGraw-Hill Book Co., Inc., New York (1962).

2. Klein, G., M. Villena-Blanco, and T. Vermeulen, Industrial Engineering Chemical Process Design Development, 3, 280-7 (1964).

3. Vermeulen, T. and N. K. Hiester, J. Chemical Physics, 22, 96 (1954).

4. Tondeur, D., and G. Klein, Industrial Engineering Chemistry Fundamentals, 6, 351 (1967).

5. Clazie, R. N., G. Klein and T. Vermeulen, University of California Sea Water Conversion Laboratory Report No. 67-4 (1967).

6. Klein, G., D. Tondeur, and T. Vermeulen, Industrial Engineering Chemistry Fundamentals, 6, 339 (1967).

7. Sillén, G. L., Arkiv Kemi 2, 477-98 (1950).

8. Vermeulen, T., G. Klein, and N. K. Hiester, Adsorption and Ion Exchange, Section 16 in Perry's Chemical Engineers' Handbook, Fifth Edition, McGraw-Hill, New York (to be published).

9. Omatete, O. O., Ph.D. Thesis in Chemical Engineering, University of California, Berkeley (1971).

10. Pandya, P. J., G. Klein, and T. Vermeulen, University of California Sea Water Conversion Laboratory Report No. 65-2 (1965).

11. Abrams, I. M. and L. Benezra, Ion Exchange Polymers, Encyclopedia of Polymer Science and Technology, Wiley (1967).

12. Klein, G., et. al., Desalination, 4, No. 2, 158-66 (1968).

13. Makar, K. M., T. Vermeulen, and G. Klein, Sea Water Conversion Laboratory Report No. 68-2 (WRC Desalination Report No. 25), University of California, Berkeley (1968).

14. Vermeulen, T. and R. E. Quilici, Industrial Engineering Chemistry Fundamentals, 9, 179 (1970).

15. Thomas, H.C., J. American Chemical Society, 66, 1664 (1944).

16. Opler, A. and N. K. Hiester, "Tables for Predicting the Performance of Fixed-Bed Ion Exchange", Stanford Research Institute, Menlo Park, California (1954).

17. Vermeulen, T., M. Nassiri, B. Nellis, and M. LeMaguer, "Fixed-Bed Sorption and Chromatography: Concentration History Tables Given by the Thomas Hiester Functions under Nonlinear Equilibrium", U. S. Office of Saline Water, in press.

18. Gilliland and Baddour, Industrial Engineering Chemistry, 45, 330 (1953).

19. Nady, L., Ph.D. Thesis in Chemical Engineering, University of California, Berkeley (1970).

LEGAL NOTICE

This report was prepared as an account of work sponsored by the United States Government. Neither the United States nor the United States Atomic Energy Commission, nor any of their employees, nor any of their contractors, subcontractors, or their employees, makes any warranty, express or implied, or assumes any legal liability or responsibility for the accuracy, completeness or usefulness of any information, apparatus, product or process disclosed, or represents that its use would not infringe privately owned rights.

TECHNICAL INFORMATION DIVISION
LAWRENCE BERKELEY LABORATORY
UNIVERSITY OF CALIFORNIA
BERKELEY, CALIFORNIA 94720